Scattering between wobbling kinks

Trabajo de Fin de Máster

Máster en Física

Autor:

João Victor Queiroga Nunes

Julio de 2020

Departamento de Física Teórica, Atómica y Óptica

Tutores:

Alberto Alonso Izquierdo (Univ. Salamanca)

Luis Miguel Nieto Calzada (Univ. Valladolid)

Scattering between wobbling kinks

J. Queiroga-Nunes[(a)], A. Alonso-Izquierdo[(b,c)], and L.M. Nieto[(a,d)]
[(a)] Departamento de Física Teórica, Atómica y Óptica, Universidad de Valladolid, 47011 Valladolid, Spain
[(b)] Departamento de Matematica Aplicada, Universidad de Salamanca, Casas del Parque 2, 37008 - Salamanca, Spain
[(c)] IUFFyM, Universidad de Salamanca, Plaza de la Merced 1, 37008 - Salamanca, Spain
[(d)] Instituto de Matemáticas (IMUVA), Universidad de Valladolid, 47011 Valladolid, Spain

July 22, 2020

Abstract

In this paper the scattering between a wobbling kink and a wobbling antikink in the standard ϕ^4 model is numerically investigated. The dependence of the final velocities, wobbling amplitudes and frequencies of the scattered kinks on the collision velocity and on the initial wobbling amplitude is discussed. The fractal structure becomes more intricate due to the emergence of new resonance windows and the splitting of those arising in the non-excited kink scattering. Outside this phase, the final wobbling amplitude exhibits a linear dependence on the collision velocity whereas the final frequency is a decreasing function. By contrast, these magnitudes are almost independent of the initial wobbling amplitude. A theoretical analysis of this new scenario is carried out by applying the collective coordinate method.

Resumen

En este artículo el scattering entre kinks y antikinks excitados mediante el modo normal de vibración de estas soluciones en el modelo ϕ^4 estándar es investigado numéricamente. La dependencia de las velocidades finales, amplitudes y frecuencias de oscilación de los kinks resultantes trás la colisión con respecto a la velocidad y amplitud inicial es analizada. La estructura fractal presente en el diagrama que proporciona la velocidad final frente a la velocidad inicial para kinks no excitados se vuelve ahora más intrincada debido al surgimiento de nuevas ventanas de resonancia. Fuera de esta fase, la amplitud final de vibración de los kinks exhibe una dependencia lineal de la velocidad de colisión mientras que la frecuencia final es una función decreciente. Asimismo, estas magnitudes son casi independientes de la amplitud de vibración inicial. El análisis teórico de este nuevo escenario es investigado aplicando el método de coordenadas colectivas.

1 Introduction

Over the last fifty years, topological defects have played an essential role in explaining a wide variety of non-linear phenomena arising in several physical contexts, including Condensed Matter [1, 2, 3, 4], Cosmology [5, 6], Optics [7, 8, 9], Molecular systems [10, 11], Biochemistry [12], etc. This broad range of applications underlies the fact that topological defects are solutions of nonlinear partial differential equations, which behave as extended particles in the physical substrate. Solitons and kinks are paradigmatic examples of this type of solutions, which have been profusely studied both in Physics and Mathematics. They arise, respectively, in the sine-Gordon and ϕ^4 field theory models, which are endowed with

two facing properties: integrability versus non-integrability. Curiously, kink scattering in non-integrable systems exhibits a richer behavior than the one found for integrable systems. The study of the collision between kinks and antikinks in the ϕ^4 model was initially addressed in the seminal references [13, 14, 15]. The complex relation between the final velocity v_f of the scattered kinks and the initial collision velocity v_0 was displayed in these papers. There exist two different scattering channels: *bion formation* and *kink reflection*. In the first case a bound state (called bion) is formed, where kink and antikink collide and bounce back over and over emitting radiation in every impact. In the second case, kink and antikink emerge after the impact and move away with a certain velocity v_f. If the initial collision velocity v_0 is low enough, a bion is always formed while for large velocities v_0 the kinks are reflected. However, the most striking feature in this scheme is that the transition between the two previously described regimes is characterized by a sequence of initial velocity windows with a fractal structure where the kinks collide several times before definitely escaping, see Figure 5. The fractal nature displayed by this final velocity versus initial velocity diagram is twofold: (a) The first two-bounce window arises approximately in the range $v_0 \in [0.1920, 0.2029]$ and it is infinitely replicated by progressively narrower windows up to the beginning of the one-bounce kink reflection regime at (approximately) $v_0 \approx 0.26$, see Figure 5. (b) Two-bounce windows are surrounded by three-bounce windows, and these ones, in turn, are surrounded by four-bounce windows, and so on. Consequently, the previously mentioned diagram displays three clearly differentiated parts: the first one corresponds to zero velocity where the bion state is formed, the second part approximately occurs in the interval [0.19,0.26], where the fractal structure emerges, and the third one refers to the 1-bounce kink reflection regime characterized by a continuous increasing curve starting at zero final velocity, which we shall call *the one-bounce tail*. Notice that there is no 1-bounce windows in the fractal region.

The presence of the n-bounce windows can be explained by means of the *resonant energy transfer mechanism*. As it is well known, the second order small kink fluctuation operator involves two discrete eigenfunctions: a zero mode (which generates an infinitesimal translational movement of the kink) and a shape mode (an infinitesimal perturbation associated with the internal vibration of the kink). The presence of these modes is the consequence of two different evolutions: (a) the kink travels with constant velocity and (b) the kink vibrates by changing its size. This last behavior defines the so-called *wobbling kink*. The previously mentioned mechanism allows an energy exchange between the zero and shape kink modes. For example, a kink and antikink could approach each other with initial velocity v_0, collide and bounce back. The impact could excite the shape mode, which would absorb a part of the kinetic energy. As a consequence, a wobbling kink and a wobbling antikink would emerge after the collision and move away. If the kinetic energy of the resulting kinks was not large enough to make the kinks escape they would end up approaching and colliding again. The new impact would cause a redistribution of the energy among the zero and vibrational modes. It is clear that the wobbling kinks play an important role in the fractal structure of the n-bounce windows. In this sense, the present study is important to understand the n-bounce scattering since after the first collision a wobbling kink and a wobbling antikink emerge with, in general, higher amplitudes than the initial one. A part of the vibrational energy could return to the zero mode making it possible for the kinks to move away and eventually escape. This describes a two-bounce kink scattering event. In general, a n-bounce event arises when the resulting kinks need to collide n times before escaping. It is worthwhile to mention that the resonant energy transfer mechanism does not arise for the soliton scattering in the sine-Gordon model. It is assumed that the reason for this is the lack of vibrational (shape) modes in this model. However, this mechanism and other related phenomena are present in a large variety of one-component scalar field theory models, such as in the double sine-Gordon model [16, 17, 18, 19, 20, 21], in deformed ϕ^4 models [22, 23, 24, 25, 26, 27, 28], in ϕ^6-models [29, 30, 31, 32, 33], and in other more complex models [34, 35]. Kink dynamics has also been analyzed in coupled two-component scalar field theory models, see [37, 38, 39, 40, 41, 42, 43, 44]. The effect of impurities, defects or inhomogeneities on kink dynamics has been discussed in several models, see references [45, 46, 47, 48, 49, 50, 51, 52, 53, 54, 55, 56, 57]. The previous description constitutes

an heuristic explanation of the resonant energy transfer mechanism, although this phenomenon has revealed to be more complicated than expected. It has been proved that it can be triggered by the discrete eigenfunctions of combined kink configuration when kink and antikink are close enough and also by quasi-normal modes [58, 59, 60]. This complexity turns the search for an analytical explanation of this phenomenon into a very elusive problem. Indeed, the collective coordinate method was initially introduced in [13] to explain the kink dynamics in the ϕ^4 model and used later to explain the resonant energy transfer mechanism in a satisfactory way. However, the presence of typographical errors in the original paper has been proved [61]. The corrected terms were not sufficient to make the collective coordinate approach fit the data outcome of the scattering process using the harmonic approximation. Recent studies [62] shows that the inclusion of more terms, up to second order, in the effective Lagrangian are necessary to make this analytical method fit with good precision the simulation data.

Other important topic in this context is the study of the evolution of the wobbling kink in the ϕ^4-model. This issue was initially discovered by Getmanov [63], who interpreted it as a bound state of three non-oscillatory kinks. Some perturbation expansion schemes have been employed to explore the properties of the wobbling kinks, see for example [64, 65, 66, 38, 50, 67]. These works show that the amplitude $a(t)$ of the wobbling mode at fourth order in the expansion decays. As a consequence the wobbling kink emits radiation. When $a(0)$ is small, the decay becomes appreciable only after long times $t \sim |a(0)|^{-2}$, see [64, 65].

In this paper we shall investigate the scattering between wobbling kinks. We think that this analysis is interesting for several reasons. The original kink scattering where the resonant energy transfer mechanism was initially discovered involves the collisions of wobbling kinks after the first impact. In other words, a n-bounce scattering process presumably includes $n-1$ wobbling kink collisions. For example, in a 2-bounce event the kinks collide and a part of the kinetic energy is transferred to the vibrational mode, such that the second collision is a wobbling kink scattering process. Indeed, this last impact causes the more (at first sight) astonishing phenomenon, the two kinks acquire more velocity than that they initially had in the second process. For this reason we think that the study of the wobbling kink scattering can bring new insight in the original problem, particularly those 1-bounce events, where the amplitude and velocity of colliding wobbling kinks can be monitored. This allows us to study the resonant energy transfer mechanism in a more direct way. Obviously, the major part of the results displayed in this paper comes from numerical analysis due to the previously mentioned fact that there are no satisfactory analytical methods to study this problem. Despite of this, we shall introduce some theoretical approaches which try to explain the numerical outcomes.

The organization of this paper is as follows: in Section 2 the theoretical background of the ϕ^4 model is introduced. The study of the kink and its linear stability leads us to the description of the wobbling kinks. The kink-antikink scattering is also discussed. Section 3 is devoted to the numerical analysis of the wobbling kink scattering. Here we shall addressed the scattering between weakly wobbling kinks and the scattering between strongly wobbling kinks in two different subsections. The distinction underlies the fact that the amplitude of the wobbling kinks decreases in the course of time. This effect is small for weakly wobbling kinks. So, we can assume in our numerical experiments that the amplitude of these kinks does not significantly change in the interval in which they are initially approaching before the collision. In Section 4 we shall try to analytically explain some of the features found in the previous section by using the collective coordinates method or by using the behavior of system invariants. Finally, some conclusions are drawn in Section 5.

2 The ϕ^4 model: Preliminaries, notation and kink-antinkink scattering

We shall deal with the ϕ^4 model in (1+1) dimensions, whose dynamics is governed by the action

$$S = \int d^2x \; \mathcal{L}(\partial_\mu \phi, \phi) \quad , \tag{1}$$

where the Lagrangian density $\mathcal{L}(\partial_\mu \phi, \phi)$ is of the form

$$\mathcal{L}(\partial_\mu \phi, \phi) = \frac{1}{2}\,\partial_\mu \phi\, \partial^\mu \phi - V(\phi) \;\; , \qquad V(\phi) = \frac{1}{2}(\phi^2 - 1)^2 \quad , \tag{2}$$

a plot of this potential and the behaviour of the static solutions can be seen in Figure 1. The use of dimensionless field and coordinates and Einstein summation convention is assumed in (1) and (2). The Minkowski metric $g_{\mu\nu}$ has been chosen as $g_{00} = -g_{11} = 1$ and $g_{12} = g_{21} = 0$. The solutions of this model verify the non-linear partial differential equation

$$\frac{\partial^2 \phi}{\partial t^2} - \frac{\partial^2 \phi}{\partial x^2} = -\frac{dV}{d\phi} = -2\phi(\phi^2 - 1) \quad , \tag{3}$$

which derives from the Euler-Lagrange equations associated with the functional (1). Static solutions solve the equation

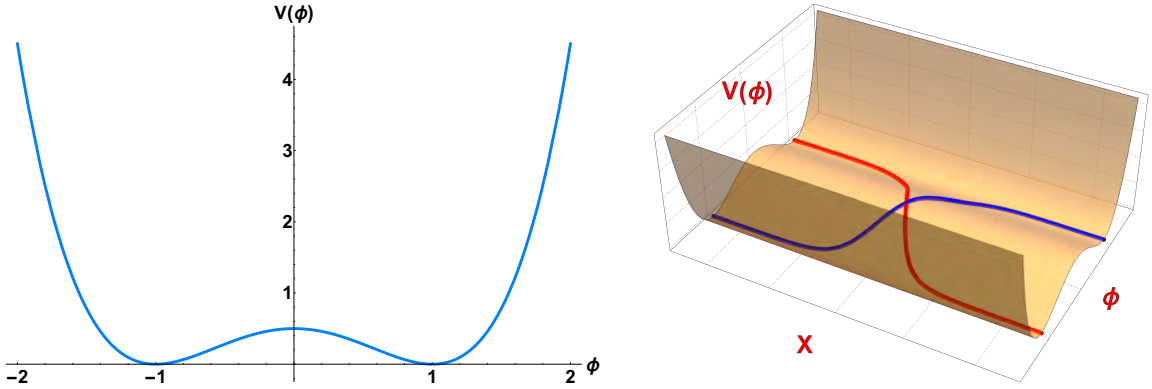

Figure 1: Potential $V(\phi)$ of the ϕ^4 model (*left*) in equation (2) and the 3D representation (*right*) of the potential with the kink (*blue line*) and antikink (*red line*) solutions connecting the minima of the potential. One can see that this potential has two minima $\mathcal{M}$ = {-1,1}, where the vacuum solutions are found to be after a spontaneous symmetry breaking.

$$\frac{d^2 \phi_s}{dx^2} = \frac{dV}{d\phi_s} \quad , \tag{4}$$

where subindex s stands for *static configuration*. Static solutions with finite energy must satisfy the boundary conditions

$$\lim_{x\to\infty} \frac{d\phi_s}{dx} = 0 \quad , \qquad \lim_{x\to\infty} \phi = \phi_s \quad . \tag{5}$$

Equation (4) can be simplified to a first order ODE by multiplying both sides by $d\phi_s/dx$ which leads us to

$$\frac{d\phi_s}{dx} = \pm\sqrt{2\,V + C} \quad . \tag{6}$$

To be in accordance with the boundary conditions (5) the constant of integration C must vanish. The energy-momentum conservation laws imply that the total energy and momentum

$$E[\phi] = \int dx \Big[\frac{1}{2}\Big(\frac{\partial\phi}{\partial t}\Big)^2 + \frac{1}{2}\Big(\frac{\partial\phi}{\partial x}\Big)^2 + V(\phi)\Big] \quad ; \quad P[\phi] = -\int dx\, \frac{\partial\phi}{\partial t}\,\frac{\partial\phi}{\partial x} \quad , \tag{7}$$

are system invariants. The integrand of the total energy $E[\phi]$ is the energy density of a configuration

$$\varepsilon[\phi(x)] = \frac{1}{2}\Big(\frac{\partial\phi}{\partial t}\Big)^2 + \frac{1}{2}\Big(\frac{\partial\phi}{\partial x}\Big)^2 + V(\phi) \quad .$$

Trivial time- and space-independent solutions of (3) are $\phi_s = \pm 1$. These solutions present null energy and identify the vacua of the model, $\mathcal{M} = \{-1, 1\}$. Non-trivial static solutions of (3) with non-null energy are of the form

$$\phi_{\rm K}^{(\pm)}(x; x_0) = \pm \tanh(x - x_0) \quad , \tag{8}$$

which are called kink/antikink $(+\,/\,-)$ and connect the two elements of the set of vacua of the potential. The kink/antikink energy density $\varepsilon[\phi_{\rm K}^{(\pm)}(x; x_0)] = \mathrm{sech}^4(x - x_0)$ is localized around the point $x = x_0$, which is assumed to be the kink center (the value where the field profile vanishes). The Lorentz invariance can be used to construct the travelling kinks/antikinks in the form

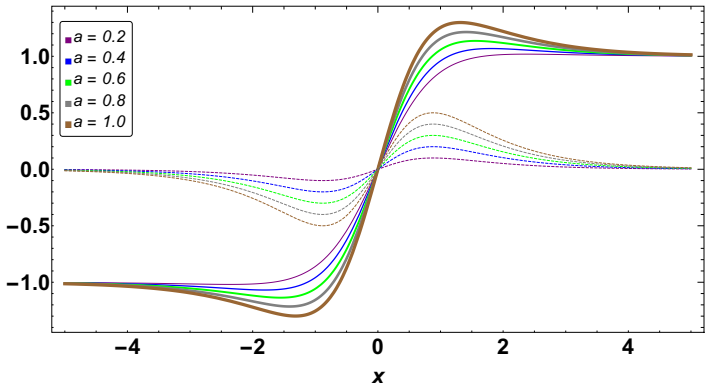

Figure 2: Kink deformed by the vibrational normal mode in first excited state for different amplitudes (*solid lines*) and eigenfunctions $\psi_{\omega^2=3}(x, x_0)$ associated to first excited mode of the ϕ^4 model (*dashed lines*).

$$\phi_{\rm K}^{(\pm)}(t, x; x_0, v_0) = \pm \tanh\left[\frac{x - x_0 - v_0 t}{\sqrt{1 - v_0^2}}\right] \quad . \tag{9}$$

Obviously, the kink center x_C for (9) moves in the real line following the expression $x_C = x_0 + v_0 t$, such that v_0 can be interpreted as the velocity of the kink center.

Now, in order to examine the linear stability of the solution, we consider fluctuations around the static kink/antikink solution (8) by adding a small perturbation as

$$\widetilde{\phi}_{\rm K}^{(\pm)}(t, x; x_0) = \phi_{\rm K}^{(\pm)}(x; x_0) + \psi(t, x; x_0) \quad . \tag{10}$$

Expanding it up to first-order in ψ into the equation of motion (3) and using the standard separation of variables ansatz

$$\psi(t, x; x_0) = a\, e^{i\omega t}\psi_{\omega^2}(x; x_0) \quad ,$$

one has the Schrödinger-like equation

$$\left[-\frac{d^2}{dx^2} + \boldsymbol{U}(x)\right]\psi_{\omega^2}(x; x_0) = \omega^2\psi_{\omega^2}(x; x_0) \quad , \tag{11}$$

where

$$\boldsymbol{U}(x) = \left.\frac{d^2V}{d\phi^2}\right|_{\phi_{\rm K}^{(\pm)}} = 4 - 6\,{\rm sech}^2(x-x_0) \quad ,$$

is named the "stability potential". In the ϕ^4 model, the term that plays the role of the Hamiltonian operator in (11) can be factorized into operators $\boldsymbol{S}_\pm = -\frac{d}{dx} \pm 2\,\phi_{\rm K}$, a condition that is enough to prove the linear stability of the kink solution. Equation (11) has one zero mode, an excited mode with eigenvalue $\omega^2 = 3$ and a continuous spectrum on the threshold value $\omega^2 = 4$, whose eigenfunctions are given by,

$$\begin{aligned}
\psi_{\omega^2=0}(x;x_0) &= {\rm sech}^2(x-x_0) = \frac{\partial \phi_K}{\partial x} \quad , \\
\psi_{\omega^2=3}(x;x_0) &= \sinh(x-x_0)\,{\rm sech}^2(x-x_0) \quad , \\
\psi_{\omega^2=4+q^2}(x;x_0) &= e^{iq(x-x_0)}[-1-q^2+3\tanh^2(x-x_0)-3iq\tanh(x-x_0)] \quad .
\end{aligned}$$

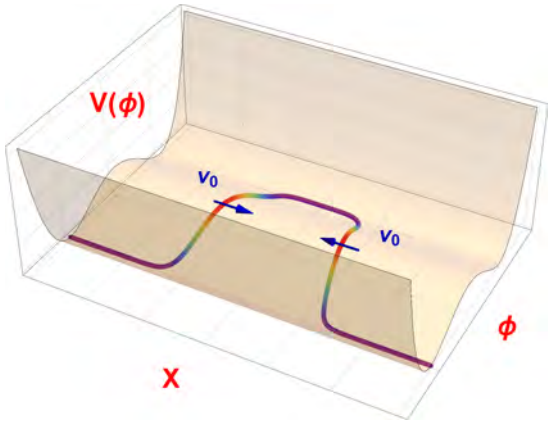

Figure 3: Configuration formed by a well separated kink and antikink, which are pushed together with initial velocity v_0.

This means that perturbations of the static kinks (10) are solutions of the nonlinear partial differential equation (3) at first order in the a-expansion. In this sense, the zero mode $\psi_{\omega^2=0}$ describes an infinitesimal translation of the static kink (8), or in other words, an infinitesimal evolution of the travelling kink (9). The shape mode $\psi_{\omega^2=3}(x;x_0)$ describes a vibrational state of the kink/antikink whose width oscillates with frequency $\omega = \sqrt{3}$. For small amplitudes a, a travelling wobbling kink/antikink $\phi_{\rm WK}^{(\pm)}$ is described by the expression

$$\phi_{\rm WK}^{(\pm)}(t,x;x_0,v_0,\omega,a) = \pm\tanh\left[\frac{x-x_0-v_0t}{\sqrt{1-v_0^2}}\right] + a\,e^{i\omega t}\sinh\left[\frac{x-x_0-v_0t}{\sqrt{1-v_0^2}}\right]{\rm sech}^2\left[\frac{x-x_0-v_0t}{\sqrt{1-v_0^2}}\right] \quad , \quad (12)$$

which is a good approximation up to first order, see Figure 2. The maximum deviation of the wobbling kink (12) from the kink (9) takes places at the points

$$x_M^{(\pm)} = x_C \pm \sqrt{1-v_0^2}\,{\rm arccosh}\,(2) \quad , \quad (13)$$

where x_C is the kink center, see Figure 2. The same result applies to the antikink. We shall analyze the evolution of the kink/antikink at these points to study the excitation of the wobbling modes in the kink scattering processes. The deviation at these points is given by

$$\left|\phi_{\rm WK}(x_M^{(\pm)}) - \phi_{\rm K}(x_M^{(\pm)})\right| = \frac{1}{2}\,|a(t)| \quad . \quad (14)$$

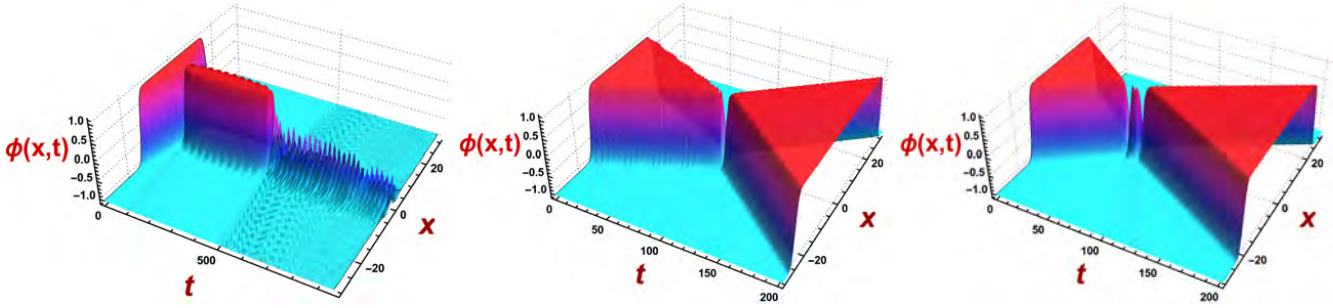

Figure 4: Bion formation (*left*), 1-bounce reflection (*center*) and 2-bounce scattering (*right*).

When the amplitude a is large enough, this magnitude can depend of the time variable. Indeed, it has been proved that the amplitude $a(t)$ of the wobbling mode at fourth order in the expansion decays the following the expression

$$|a(t)|^2 = \frac{|a(0)|^2}{1+\omega\,\xi_I\,|a(0)|^2 t} \quad , \tag{15}$$

where ξ_I is a constant. When $a(0)$ is small, the decay becomes appreciable only after a long time $t \sim |a(0)|^{-2}$, see [64, 65].

The scattering between a kink and an antikink (whose shape eigenfunctions are unexcited, i.e. $a = 0$ in (12)) has been thoroughly analyzed in the physical and mathematical literature. In this case, a kink and antikink, which are well separated, are pushed together with initial collision velocity v_0. Taking into account the spatial reflection symmetry of the system, the kink can be located at the left of the antikink or viceversa. This configuration can be characterized by the concatenation

$$\phi_K^{(\pm)}(t,x,x_0,v_0,\omega,0) \cup \phi_K^{(\mp)}(t,x,-x_0,-v_0,\omega,0) = \begin{cases} \text{if } \; x<0, & \phi_{\rm K}^{(\pm)}(t,x,x_0,v_0,\omega,a) \\ \text{if } \; x\geq 0\,, & \phi_{\rm K}^{(\mp)}(t,x,-x_0,-v_0,\omega,a) \end{cases} \quad , \tag{16}$$

for $x_0 \gg 0$, see Figure 3. Two different scattering channels have been found in this situation:

1. *Bion formation*: In this case, kink and antikink approach each other, then collide and bounce back. After the impact an exchange of energy from the translational mode to the shape and continuous modes takes place in such a way that the kinetic energy of these two kinks is not big enough to make them escape. Therefore, they approach each other again, collide and bounce back over and over. This is a long living bound kink-antikink state called bion.

2. *Kink reflection*: Now, kink and antikink approach each other, collide and bounce back. After the impact a redistribution of the energy among the normal modes occurs. After colliding a finite number n of times, kink and antikink emerge and move away with final velocity v_f. These processes will be referred to as n-bounce scattering events, see Figure 4.

If we plot the final velocity of the scattered kinks as a function of the initial collision velocity v_0 we find the diagram displayed in Figure 5. Here, it is assumed that the final velocity for a Bion state is zero. It is clear that the bion formation regime arises for low enough values of the collision velocity v_0. On the other hand, if v_0 is greater than 0.25988 then kink and antikink reflect each other after colliding once (blue curve in Figure 5). We will referred to this piece of curve as *the one-bounce tail*. Note that a color code has been used in Figure 5 to specify the number of collisions that the kinks suffer before escaping. A surprising fractal pattern turns up in the interval $[0.18, 0.25988]$, where the bion formation and kink reflection regimes are interlaced. The red curves (which characterize 2-bounces events) are

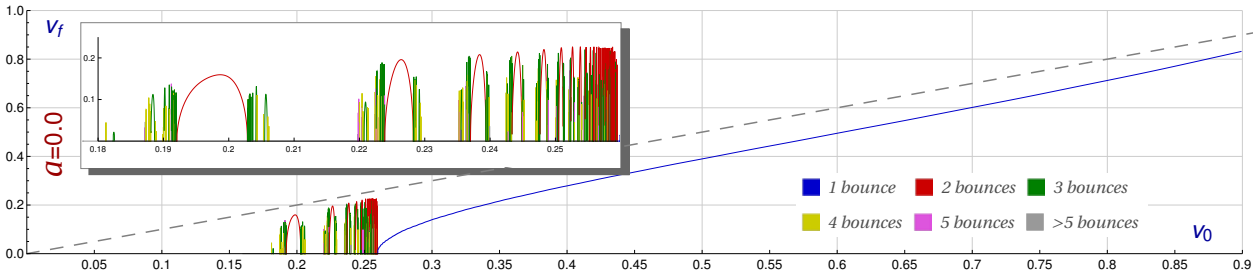

Figure 5: Final velocity v_f of the scattered kinks as a function of the initial collision velocity v_0 of the colliding kinks. The final velocity of a Bion is assumed to be zero. The color code is used to specify the number of bounces suffered by the kinks before escaping. The resonance window has been zoomed and inserted in the Figure.

surrounded by green curves (which determine 3-bounces processes) and so on. Besides, this scheme is infinitely replicated as we approach the one-bounce reflection kink regime, see zoomed area in Figure 5.

It is worthwhile to mention that after the first collision in a n-bounce scattering process the following collisions involve wobbling kinks due to the fact that the first impact usually excites the shape mode of the initially colliding kinks. It is difficult to monitor the velocities and amplitudes of the resulting kinks after the first impact in an n-bounce event because the period of time between bounces is usually very short. For this reason it seems reasonable to directly investigate the collision between wobbling kinks. In this situation the velocity and amplitude of the colliding and scattered wobbling kinks can be monitored, at least, in the one-bounce processes. In any case, this type of scattering events can provide us with a lot of information about the resonant energy transfer mechanism.

3 Scattering between wobbling kinks

The goal of this paper is to analyze the scattering between wobbling kinks. In order to accomplish this task we shall employ numerical approaches based on the discretization of the partial differential equation (3). In the collision process between wobbling kink and wobbling antikink the energy transfer mechanism takes place and part of energy interchanged between normal modes is released to space as radiation. When this radiation reach the edges of the grid it is reflected back to the center of the grid if no appropiate boundary conditions are considered and this could disrupt the interaction between the topological defects, see Figure 6. For this reason, the numerical procedure used in this paper corresponds to an energy conservative second-order finite difference algorithm implemented with Mur boundary conditions. The effect of radiation in the simulation is controlled by this algorithm because the linear plane waves are absorbed at the boundaries. As a complement to this numerical method has also been employed the algorithm described in [68] by Kassam and Trefethen. This scheme is spectral in space and fourth order in time and was designed to solve the numerical instabilities of the exponential time-differencing Runge–Kutta method introduced in [69]. The initial settings for our scattering experiments are described by two initially well separated wobbling kinks which are pushed together with initial collision velocity v_0. This situation is characterized by the concatenation

$$\phi^{(\pm)}_{\mathrm{WK}}(t,x,x_0,v_0,\omega,a) \cup \phi^{(\mp)}_{\mathrm{WK}}(t,x,-x_0,-v_0,\omega,a) = \begin{cases} \text{if } \; x \geq 0, & \phi^{(\pm)}_{\mathrm{WK}}(t,x,-x_0,-v_0,\omega,a) \quad , \\ \text{if } \; x < 0, & \phi^{(\mp)}_{\mathrm{WK}}(t,x,x_0,v_0,\omega,a) \quad , \end{cases} \tag{17}$$

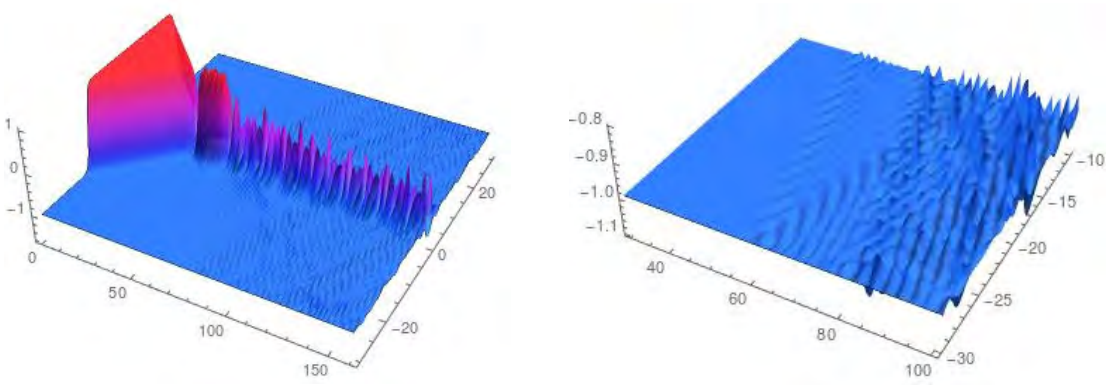

Figure 6: During the exchange of energy between normal modes of the topological defects a small amount of energy is released as radiation to space. Without good boundary conditions, this radiation reflect back to the center of grid and disrupt the evolution of the scattering process. A bion formation (*left*) and the reflection of radiation at the edges of the grid (*right*) is shown above.

where $x_0 \gg 0$ and

$$\phi_{\rm WK}^{(\pm)}(t,x;x_0,v_0,\omega,a) = \pm \tanh\left(\frac{x-x_0-v_0t}{\sqrt{1-v_0^2}}\right) + a\,\sin(\omega t)\,\mathrm{sech}\left(\frac{x-x_0-v_0t}{\sqrt{1-v_0^2}}\right)\tanh\left(\frac{x-x_0-v_0t}{\sqrt{1-v_0^2}}\right), \tag{18}$$

has been chosen to comply with the initial condition $\phi_{\rm WK}^{(\pm)}(0,x;x_0,v_0,\omega,a) = \phi_K^{(\pm)}(t,x,x_0,v_0)$, see Figure 3. The configuration (17) consists of a wobbling kink/antikink with center $-x_0$ located at the left side of an wobbling antikink/kink with center x_0. It is clear that if $x_0 \gg 0$ and $a \ll 1$ the partial differential equation (3) is verified by (17) very approximately. The initial conditions for our problem can be derived from (17) by simply taking $t = 0$, that is, $\phi(0,x;x_0,v_0,\omega,a)$ and $\frac{\partial\phi}{\partial t}(0,x;x_0,v_0,\omega,a)$ define the starting point of the numerical algorithm. Note that the configuration (17) is invariant under the spatial reflection transformation $x \mapsto -x$, as it is also the evolution equation (3), so all the scattering processes will preserve this symmetry. This means that we can extract all the scattering information by analyzing the features of only one of the scattered kinks. In particular, our numerical experiments have been carried out in a spatial interval $x \in [-100, 100]$ where the kink and the antikink centers are initially separated by a distance $d = 2x_0 = 60$. These kink centers have been monitored during the evolution, as well as the number of bounces suffered by the topological defects. In the kink reflection regime this information is used to work out the final velocity of the scattered kinks by employing a linear regression when the kinks are far enough apart from each other. Moreover, the time interval $t \in [0, t_{max}]$ of the simulation depends on the initial velocity of the wobbling kink/antikink. If the initial velocity is smaller than 0.3 the $t_{max} = 900 + 15/v$, otherwise, $t_{max} = 190 - 131/v + 85/v^2$. We argue that for initial velocities bigger than 0.3 the 1-bounce reflection process are most likely to emerge then, a shorter time interval of computation is enough to cover all the scattering process. This scheme has been performed for a range of initial velocities v_0 usually covering the interval $v_0 \in [0.1, 0.9]$ with initial velocity steps $\Delta v_0 = 0.001$, which is decreased to $\Delta v_0 = 0.00001$ in the resonance range. Although, as the initial velocity approach the end of the fractal regime, the resonance windows get narrower, see Figure 5, and even for initial velocity steps $\Delta v_0 \ll 1$ is possible that some resonance windows may not appear. These data allow us to study the dependence of the separation velocity of the scattered kinks as a function of the collision velocity v_0, which can be graphically represented by means of diagrams similar to Figure 5. Once the position and the velocity of the kink centers have been determined the wobbling amplitude and frequency are also estimated. To do this, the difference between the numerical profile and a non-excited traveling kink, both of them with the same center x_C and velocities v_f is evaluated at the points $x_M^{\pm}$ for every

time step in the simulation. The choice of these points underlies the fact that the wobbling fluctuation has its maximum/minimum values at the points $x_M^{\pm}$. The time series constructed in this way is analyzed by using a fast Fourier transform algorithm.

In order to explore the dependence of the final velocity on the initial wobbling amplitude of the colliding kinks the previously described numerical scheme has been replicated for different values of the amplitude a considered in the initial configuration. In these numerical experiments we shall consider only positive values of a. Negative values of a are simply related with the positive ones by adding a phase in the argument of the oscillatory factor $\sin(\omega t)$ in (18). To get a better understanding of the phenomena associated with this type of scattering processes is convenient to distinguish two different regimes which depend on the magnitude of the amplitude a. They are determined as follows:

1. *Scattering between weakly wobbling kinks:* This scenario comprises those scattering processes where the initial amplitude a of the colliding wobbling kinks is $|a| < 0.05$. In these cases the amplitude decay effect is assumed to be negligible such that the wobbling amplitude of the evolving kinks at the time of impact is approximately equal to the initial one. It is clear that this kind of events allows a better control on the variables of the scattering problem. The mechanisms that begin to deform the velocity diagram with respect to the pattern found in Figure 5 when a is increased can already be perceived in these cases. These novel behaviors will be discussed in Section 3.1.

2. *Scattering between strongly wobbling kinks:* It is expected that the more intense phenomena take place when the wobbling amplitudes of the colliding kinks are relatively large. We assumed that these cases are determined by the condition $|a| \geq 0.1$. Now, the amplitude decay suffered by the wobbling kinks in the time period lapsed between the beginning of the simulation and the kink collision (approximately $d/(2v_0)$) could be significant. Therefore, it is difficult to estimate the value of the wobbling amplitude immediately before the impact, which is from our point of view the more significant variable. Despite this fact this type of events plays an essential role in the resonance mechanism and for this reason it will be discussed in Section 3.2. We shall analyze the dependence of some scattering parameters on the initial wobbling amplitude of our numerical experiments taking into account that the value of the collision amplitude will be smaller than the initial one. Obviously, the higher the initial magnitude is the higher the collision amplitude is.

3.1 Scattering between weakly wobbling kinks

In this section, we shall consider the scattering of kinks whose initial wobbling amplitudes a are small. As previously mentioned it is assumed that in these cases the decay of the wobbling amplitude is a residual effect. Thus, the magnitude of the wobbling amplitude of the kinks just before colliding must be approximately equal to the initial one. This first regime of kink scattering has been numerically investigated in the initial wobbling amplitude range $a \in [0, 0.05]$ taking an amplitude step $\Delta| = 0.001$ for $0 \leq |a| \leq 0.02$ and $\Delta a = 0.01$ for $a > 0.02$. A characteristic velocity diagram obtained is displayed in Figure 7, where the dependence of the final velocity v_f of the scattered kinks on the initial collision velocity v_0 is graphically represented when the initial wobbling amplitude is $a = 0.02$. Although this value is relatively small the diagram displayed in Figure 7 introduces novel features with respect to the classical diagram presented in Figure 5.

It can be observed that the complexity of the fractal structure grows as the initial wobbling amplitude a increases. A first sign of this fact is that the fractal structure interval is widened as a increases. For example, this interval is approximately $[0.155, 0.277]$ for the case $a = 0.02$ whereas it is approximately $[0.18, 0.26]$ for the case $a = 0$. A second indicator is the growth in the number of resonance windows. Indeed, this effect is caused by a resonance window splitting mechanism, which is illustrated in Figure 8. Before examining this process it is worthwhile to bring our attention to another novel property of

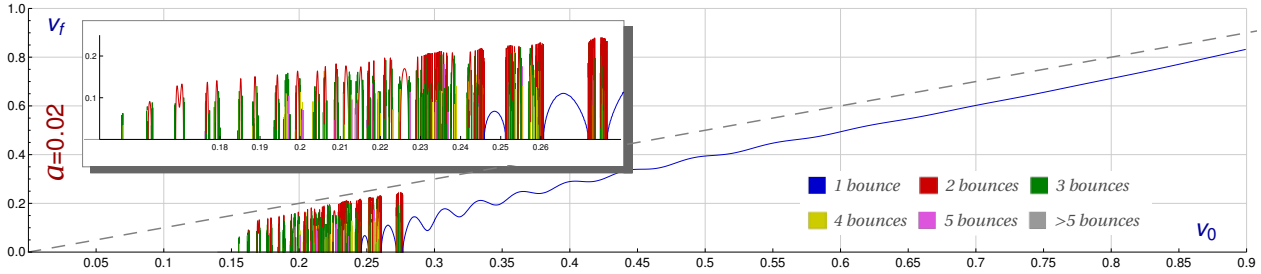

Figure 7: Final velocity v_f of the scattered kinks as a function of the initial collision velocity v_0 of the colliding wobbling kinks with initial amplitude $a = 0.02$. The final velocity of a Bion is assumed to be zero. The color code is used to specify the number of bounces suffered by the kinks before escaping. The resonance window has been zoomed and inserted in the Figure.

the diagram in Figure 7: the presence of isolated 1-bounce windows in the fractal structure, which, in turn, are surrounded by other n-bounce windows with $n \geq 2$. This feature does not arise in the classical velocity diagram with zero initial energy on the shape mode displayed in Figure 5 and its origin seems to be produced by two different procedures. Figure 7 shows the existence of two isolated 1-bounce windows approximately in the intervals $[0.246, 0.251]$ and $[0.261, 0.272]$, each of them generated by different channels. They are described as follows:

1. *1-bounce reflection tail splitting*: This process is based on the oscillatory behavior of the 1-bounce tail arising for large initial velocities and represented by blue curves in Figures 5 and 7. For $a = 0$ this 1-bounce tail is a monotonically increasing function, see Figure 5. However, this curve ceases to follow that behavior and begins to oscillate as the amplitude a grows, see Figure 7. The amplitude of these oscillations becomes bigger as the value of a grows, overall at the beginning of the 1-bounce tail. When the amplitude a is large enough the minima of the previously mentioned oscillations can intercept the v_0-axis, reaching a zero final velocity. As a consequence an isolated 1-bounce window arises and the gap between this window and the 1-bounce tail is filled with new n-bounce windows. This phenomenon can be triggered repeatedly as a increases giving rise to several isolated 1-bounce windows embedded in the resonance regime. The previously described mechanism can be visualized in Figure 8, where the final velocity versus initial velocity diagrams have been plotted for the three close initial amplitudes $a = 0.013$, $a = 0.014$ and $a = 0.015$. We can observe the formation of an isolated 1-bounce window approximately in the interval $v_0 \in [0.26, 0.273]$.

2. *Spontaneous emergence in the resonance phase*: The other process, instead, is characterized by the appearance of windows inside the resonance interval. In these new windows the wobbling kinks collide only once before escaping. The explanation for this fact seems to be that the additional energy carried by the excited kinks in these scattering events due to shape mode allows the kinks to escape in initial velocity windows where this was not possible before. For example, the formation of the first window of this kind happens approximately for $a = 0.011$ around the value $v_0 = 0.249$. As the value of a increases the width of these windows widens. Indeed, this first window can be observed in Figure 8 for the initial amplitudes $a = 0.013$, $a = 0.014$ and $a = 0.015$. The second window of this class arises for $a = 0.030$ around $v_0 = 0.233$. From here the number of the windows grows enormously, see Figure 9.

Figure 9 illustrates the combined effect of the previously mentioned processes of production of isolated 1-bounce reflection windows. This figure shows the evolution of the velocity diagrams associated to 1-bounce events as the initial wobbling amplitude a increases from $a = 0$ (red curve) to $a = 0.1$ (dark blue curve). For the sake of clarity, n-bounce processes with $n \geq 2$ are not included in this graphics. Together to the reflection tail splitting and the spontaneous emergence processes another curious behavior

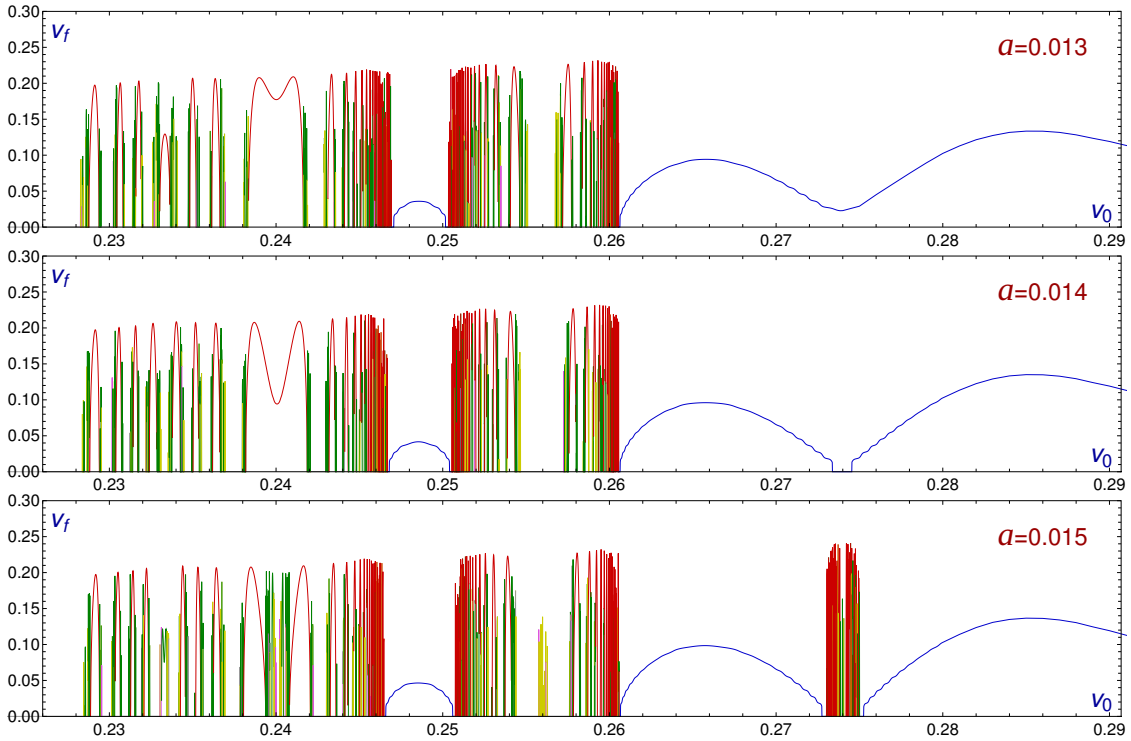

Figure 8: Velocity diagrams for the wobbling kink scattering with initial amplitudes $a = 0.013$, $a = 0.014$ and $a = 0.015$ for the initial velocity interval $v_0 \in [0.2260, 0.2907]$. This sequence of graphics illustrates the formation of isolated 1-bounce windows and the 2-bounce window splitting mechanism.

is displayed in Figure 9. The oscillations of the final versus initial velocity curves for the different values of the amplitude a have common nodes. They intersect each other at the same points (at least in a large degree of approximation).

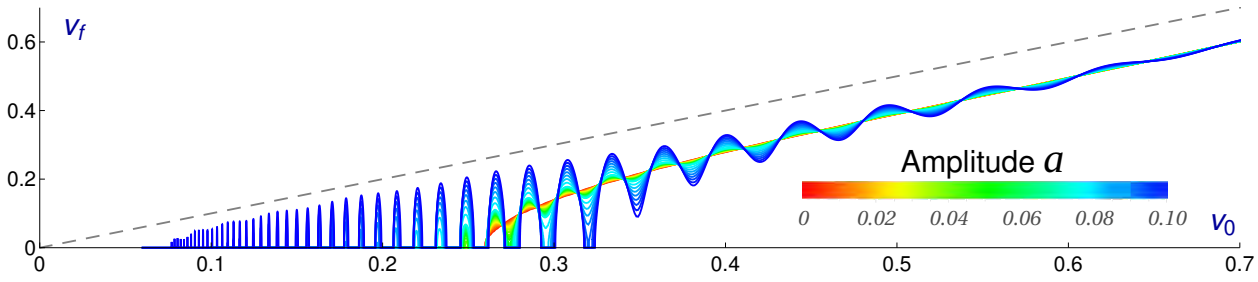

Figure 9: Velocity diagram associated with 1-bounce scattering events for initial wobbling amplitudes ranging in the interval $a \in [0, 0.10]$. This graphics illustrates the formation of isolated 1-bounce windows. For the sake of clarity, n-bounce procesees with $n \geq 2$ have not been included in this figure.

Now, let us return to the previously mentioned resonance window splitting mechanism. If we observe Figure 8 around the initial velocity $v_0 = 0.24$, we will witness the split of a 2-bounce window into other two narrower 2-bounce windows. As before, the gap between these two new 2-bounce windows is occupied by new n-bounce windows with $n > 2$. To emphasize the behavior of this newfangled feature the evolution of the first 2-bounce window found in the classical velocity diagram for $a = 0$ (see Figure 5) as the value of the wobbling amplitude a increases is shown in Figure 10. It can be observed that the initial 2-bounce window $v_0 \in [0.1920, 0.2028]$ (represented by a red curve) gives rise to three new 2-bounce windows $v_0 \in [0.1940, 0.1946]$, $v_0 \in [0.1990, 0.1998]$ and $v_0 \in [0.2039, 0.2046]$ (represented by

blue curves) for $a = 0.02$. This process is repeated for the majority of the resonance windows as the initial wobbling amplitude grows escalating the complexity of the fractal pattern in the resonance phase.

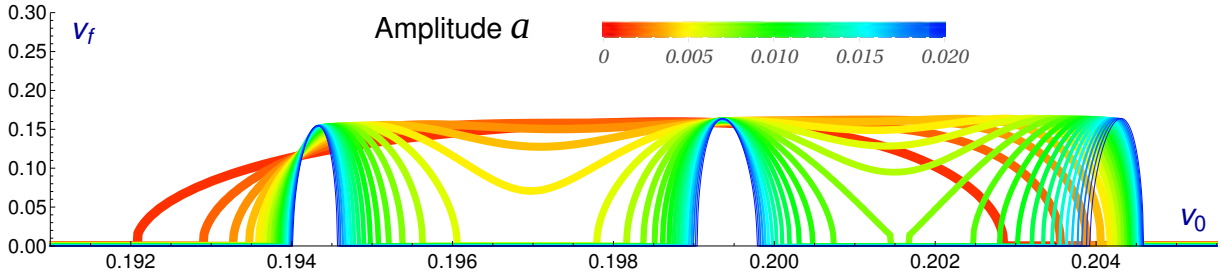

Figure 10: Evolution of the first 2-bounce window found in the velocity diagram for $a = 0$ (*red curve*) as the value of the initial wobbling amplitude increases up to $a = 0.02$ (*dark blue curves*). For the sake of clarity only 2-bounce scattering events have been included in this graphics.

Note that the formation of isolated 1-bounce windows leads to an ambiguity in the concept of the *critical velocity* v_c. This term was introduced in the context of kink-antikink scattering [14, 18] and was defined as the lowest velocity at which the 1-bounce reflection regime takes place, or alternately, the lowest velocity at which the 1-bounce tail starts and no more bion states or more multi-bounces are observed. These two definitions coincide when the two colliding kinks are not wobbling because there is only one (blue) piece of 1-bounce curve, see Figure 5, but they can differ in other cases. In order to remove this ambiguity we shall distinguish these two velocities, referring to the first one as the *1-bounce reflection minimum escape velocity* v_r whereas the second one will be called *1-bounce tail minimum escape velocity* v_t. Since more energy in the vibrational mode means that more energy can be released to the translation mode in the scattering process through the resonant energy transfer mechanism, it is expected that 1-bounce windows become more prevalent as the value of the wobbling amplitude a grows. Consequently, it is presumed that the velocity v_r is a decreasing function of the amplitude a. On the other hand, the isolated 1-bounce window formation previously explained implies that the velocity v_t must grow as the amplitude a increases. In the transition from initial amplitude $a_0 = 0$ to $a_0 = 0.014$ the escape velocity v_t is observed to increase logarithmically, however, this pattern is broken by the existence of a discontinuity due to the formation of the first isolated 1-bounce window from the reflection tail.

After discussing the features of the velocity diagram as a function of the initial amplitude a, we shall illustrate some particular processes. In Figure 11 (left) a wobbling kink and a wobbling antikink with collision velocity $v_0 = 0.285$ and initial amplitude $a = 0.02$ approach each other, collide, bounce back and move away with final velocity $v_f = 0.144805$ and wobbling amplitude $a_f = 0.175462$ after the collision. These dynamical parameters are the same for the kink and the antikink, in agreement with spatial reflection symmetry. Once they do not collide back after the first bounce the energy stored in the vibrational mode remains there and propagates within the kinks. The process displayed in Figure 11 (right) describes a 3-bounce event with initial velocity $v_0 = 0.25737$ and amplitude $a = 0.02$. In this case, the scattered kink and antikink travel away with velocity $v_f = 0.219$ and wobbling amplitude $a_f = 0.003085$. We can see the resonant energy transfer mechanism in action in these cases. In the 1-bounce event the outcome amplitude a_f is bigger than the initial amplitude a, which evinces an energy transfer from the translational mode to the shape mode being the final separation velocity v_f less than the initial one v_0. On the other hand, in the 3-bounce process this mechanism takes place three times redistributing the energy between the kinetic and vibrational energy pools after every collision. Clearly, in the first impact the shape mode gains energy at the expense of the zero mode, which finally recovers part of that energy in the third collision allowing the kinks to escape. Note that radiation emission is also involved in these processes.

In Figure 12 we have decided to illustrate the behavior of two extreme scattering events, which are

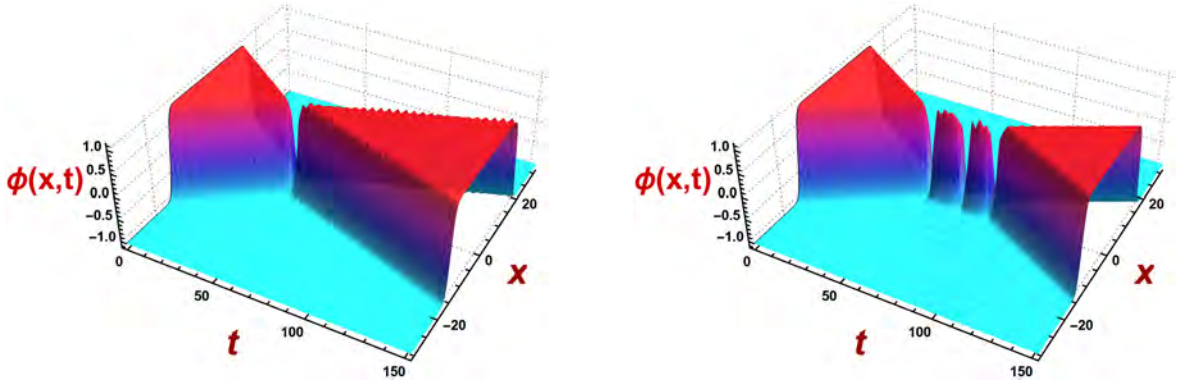

Figure 11: Scattering processes between two wobbling kinks with initial amplitude $a_0 = 0.02$ and collision velocities $v_0 = 0.25737$ (left) and $v_0 = 0.295$ (right). The final velocities and wobbling amplitudes for these events are, respectively, $v_f = 0.144805$, $a_f = 0.175462$ and $v_f = 0.219$, $a_f = 0.003085$.

near to metastable configurations. In the first process, left plot, kink and antikink approach each other with initial velocity $v_0 = 0.24691$ and wobbling amplitude $a = 0.013$, collide and bounce back. For a long time, they apparently remain motionless at a fixed distance. In this particular simulation this situation takes approximately 400 time units in the dimensionless coordinates introduced in Section 2. Finally, the lumps end up approaching again to form a bion state. In the second simulation Figure 12 (right) the kinks initially travel with velocity $v_0 = 0.27420$ and wobbling amplitude $a = 0.015$; after colliding the kink and antikink remain in a similar quasi-metastable estate which was previously described, although in this case after the second collision the kinks are able to escape with final velocity $v_f = 0.147041$ and wobbling amplitude $a_f = 0.15351$. This type of scattering events are difficult to monitor because there will always be processes whose metastable phase will last more than any simulation time. Indeed, this is the reason for the gap in the velocity diagram introduced in Figure 8 (middle) around $v_0 = 0.274$.

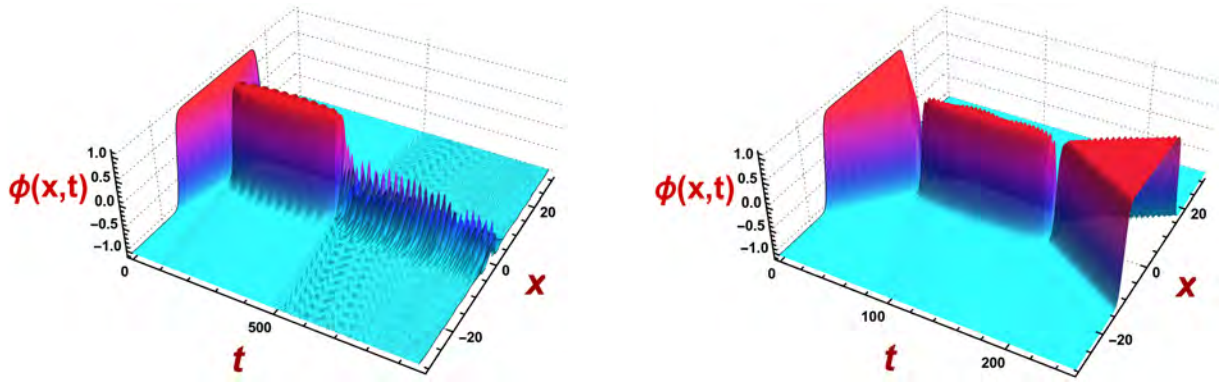

Figure 12: Scattering processes between two wobbling kinks with initial velocities and amplitudes $v_0 = 0.24691$, $a = 0.013$ (left) and $v_0 = 0.27420$, $a = 0.015$ (right). In the first case a bion state is formed whereas in the second case the scattered kinks have $v_f = 0.147041$ and $a_f = 0.15351$.

Clearly, in the previous simulations the wobbling mode is strongly excited after the first collision. This is a general pattern as we can observe in Figure 13, which exhibits the final wobbling amplitude of the scattered kinks after the last collision as a function of the initial velocity v_0 for two different values of the initial wobbling amplitude $a = 0.0$ and $a = 0.02$. The analysis of these data, specially for the 1-bounce events, can lead to a very valuable information to understand the resonant energy transfer mechanism. 1-bounce events can be considered as elementary processes in the kink scattering because n-bounce events can be understood as a reiteration of n+1-bounce events. The most surprising

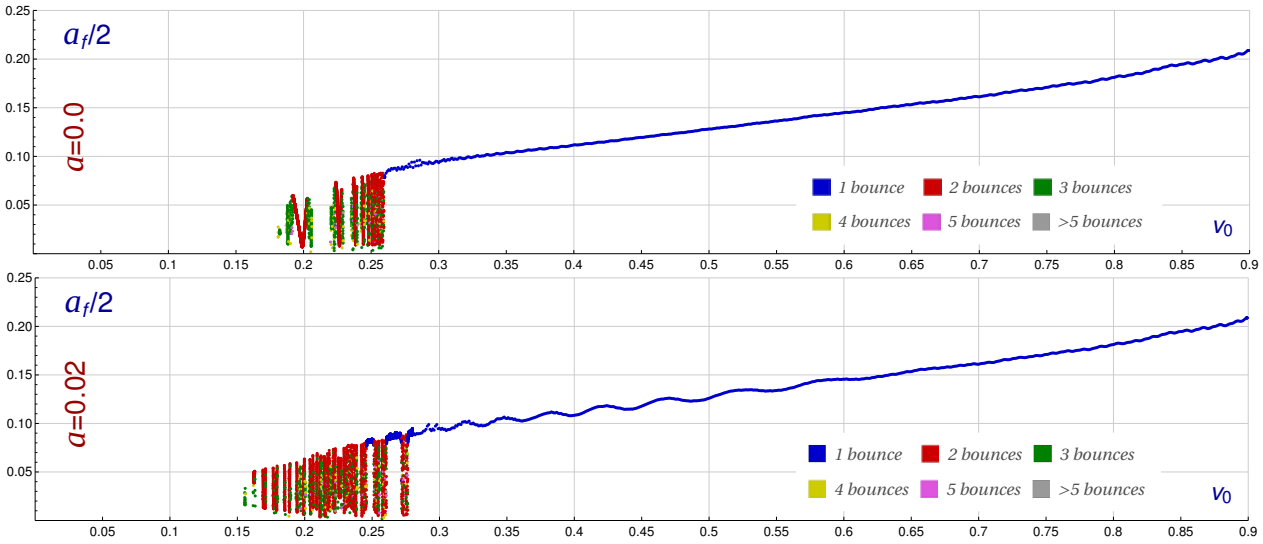

Figure 13: Wobbling amplitude a_f of the scattered kinks after the last impact as a function of the collision velocity for the initial amplitude $a = 0$ (top panel) and $a = 0.02$ (bottom panel). The same color code employed in the previous figures is used to specify the number of bounces suffered by the kinks before escaping.

fact is that the final amplitude for the 1-bounce processes is almost independent of the initial wobbling amplitude of the colliding kinks. We can observe that this magnitude follows a linear dependence on v_0 very approximately, which can be fitted by the expression

$$a(v_0) = 0.084 + 0.34 v_0 \quad . \tag{19}$$

What is clear from Figure 13 is that all the 1-bounce events produce a strong excitation of the wobbling mode, which in all the cases range approximately in the interval $a_f \in [0.15, 0.4]$. Obviously, the more the impact velocity of the colliding kinks is, the more excited the scattered kinks become. For moderate collision impact the final wobbling amplitude is in the range $a_f \in [0.15, 0.25]$. A first consequence of this high vibrational excitation in 1-bounce scattering events for initially weakly wobbling kinks is that the n-bounce events in this regime necessarily involve the scattering of strongly wobbling kinks in one or several of the intermediate collision processes (at least in the second one). A second consequence is that the direction of energy transfer in these 1-bounce events is always from the kinetic energy to the vibrational energy. Notice that the final velocity v_f of the scattered kinks in 1-bounce events displayed in Figure 7 is always less than the initial velocity v_0. The isolated 1-bounce windows found in this regime proves that there exist some initial velocity intervals where less energy is transferred to the shape mode, which allows the kinks keep enough kinetic energy to escape. The reverse processes must involve the scattering between strongly wobbling kinks.

Another surprising result is given by the dependence of the wobbling frequency ω_f of the scattered kinks on the collision velocity v_0. Note that the shape mode coming from the second order small kink fluctuation operator expressed in (11) vibrates with the frequency $\omega = \sqrt{3}$. It would seem reasonable to assume that this frequency is kept constant at least by the time the scattered kinks are far away. Figure 14 shows this magnitude as a function of the initial velocity v_0. It can be observed that the final wobbling frequency ω_f is a decreasing function on the variable v_0, which goes from the value $\sqrt{3}$ for small values of v_0 and arrives approximately to 0.865 at $v_0 = 0.9$ in the graphics. The previously supposed behavior is confirmed only for values of $v_0 < 0.4$. For greater values of v_0 the scattered kinks vibrate slower. It is difficult to provide a reason for this behavior. It could be a behavior of the wobbling kinks when they are traveling away at high velocities or it could be caused exclusively by the impact. Recall that the spectral analysis of the wobbling mode requires to study its evolution for a large enough lapse of time.

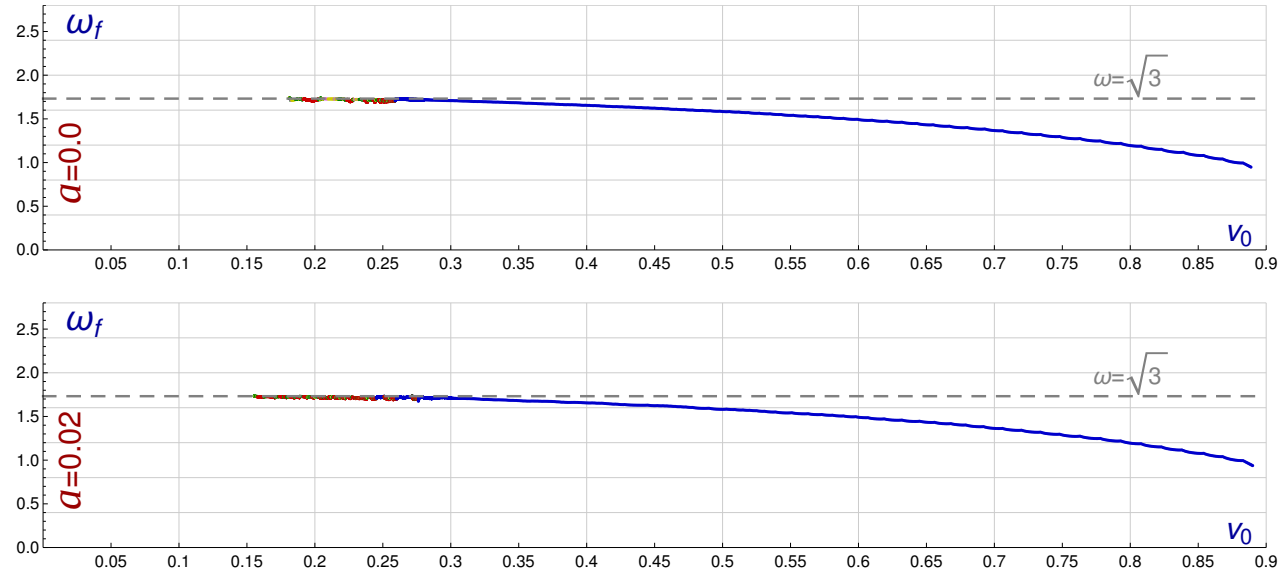

Figure 14: Wobbling frequency of the scattered kinks after the last impact as a function of the collision velocity for the initial amplitude $a = 0$ (top panel) and $a = 0.02$ (bottom panel). The same color code employed in the previous figures is used to specify the number of bounces suffered by the kinks before escaping.

Other remarkable fact is that the two graphics in Figure 14 are almost identical, which implies that the behavior of the final frequency is practically independent of the initial wobbling amplitude a for the cases presented in this Section.

As previously mentioned in this Section, the scattering between strongly wobbling kinks is always present in the resonance phenomenon because independently of the initial velocity v_0 the second collision will involve a strongly wobbling kink scattering event. For this reason the next section will be devoted to discuss the properties of this kind of more violent events. We shall emphasize the deviations of this new scenario from that introduced in this section.

3.2 Scattering between strongly wobbling kinks

This class of kink scattering processes are characterized by a relatively large value of the initial wobbling amplitude, which is assumed to be $|a| \geq 0.1$. In this section this regime has been analyzed for events with an initial amplitude a in the interval $a \in [0.1, 0.2]$ by taking an amplitude step $\Delta a = 0.01$. As usual we shall begin by examining the dependence of the final velocity v_f of the scattered kinks on the initial velocity v_0. This function has been plotted in Figure 15 for the particular cases $a = 0.1$ and $a = 0.2$, which exhibit the representative properties of this regime. The global behavior of these velocity diagrams is similar to that described in Section 3.1, see Figure 7, although they include important differences.

First, the fractal structure becomes even more intricate than the scenario found in Section 3.1. The interval where the resonance phenomenon takes place keeps widening as a grows. In addition to this, when the value of a is large enough the number of isolated 1-bounce windows explodes and the sequence of these windows forms a fractal structure clustered near the origin of the graphics, see bottom panel in Figure 15. The initial velocities v_0 around the peak of these windows can define initial velocity intervals where the scattered kinks move faster than the colliding kinks, $v_f > v_0$. In these cases a part of the vibrational kink energy accumulated in the shape mode is transferred to the kinetic energy, which becomes bigger than its initial value. It can be observed that this phenomenon occurs for low initial velocities and ceases to happen for high values (when the kinetic energy is large). For example, for $a = 0.2$ the height of the windows in the resonance phase exceeds the elastic limit approximately when

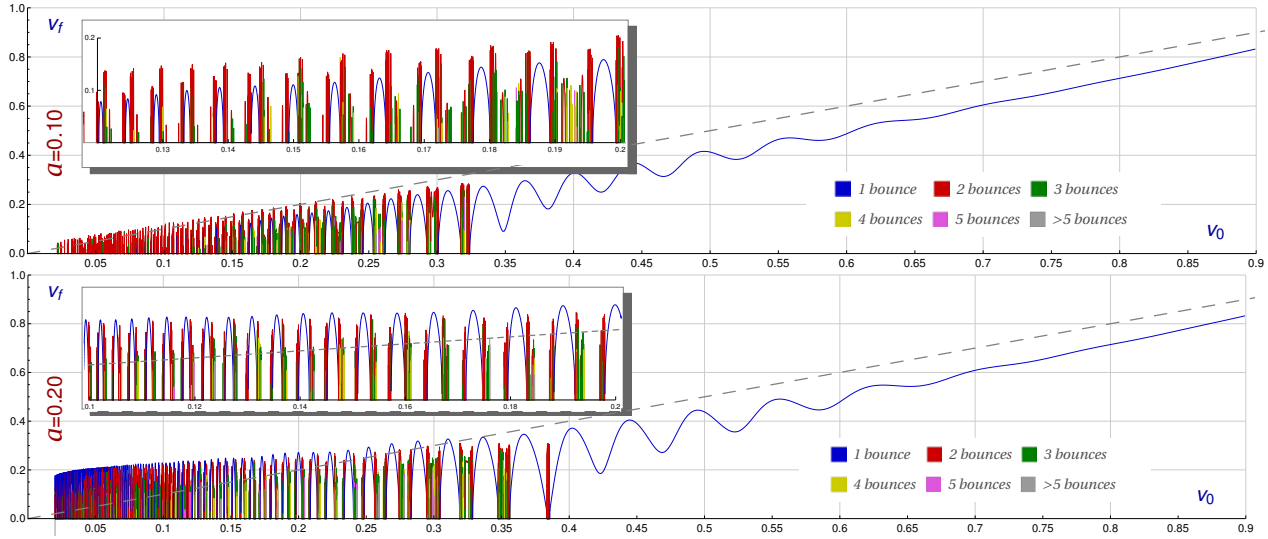

Figure 15: Final velocity v_f of the scattered kinks as a function of the initial collision velocity v_0 of the colliding wobbling kinks with initial amplitudes $a = 0.1$ (top panel) and $a = 0.2$ (bottom panel). The final velocity of a Bion is assumed to be zero. The color code is used to specify the number of bounces suffered by the kinks before escaping. The part of the resonance window has been zoomed and inserted in the Figure.

$v_0 < 0.34$. Obviously, as the value of the initial amplitude a increases this threshold velocity grows because the vibrational energy becomes bigger. This scenario is a fundamental link in the chain of the resonant energy transfer mechanism because allows relatively slow scattered wobbling kinks to escape in a multiple bounce event in the last collision by transferring vibrational energy to the kinetic energy pool. Figure 16 illustrates this kind of processes. In this graphics a kink and antikink with initial velocity $v_0 = 0.1506$ and wobbling amplitude $a = 0.2$ approach each other and collide only once before escaping. As we can see, the scattered kink and antikink move away with final velocity $v_f = 0.246454$ while its wobbling amplitude is approximately $a = 0.0215$. The final outcome in this event is that the kink and antikink are speeded up whereas its wobbling is softened.

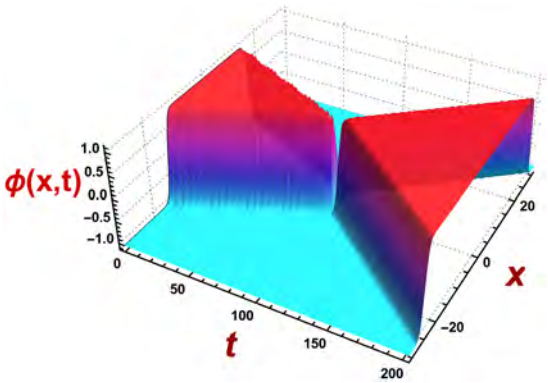

Figure 16: Scattering between two wobbling kinks with initial amplitude $a_0 = 0.2$ and collision velocity $v_0 = 0.1406$. The final velocity v_f of the scattered kinks is $v_f = 0.246454$, so the kinks move faster after the collision.

Figure 12 (right) represents a 2-bounce kink scattering process, which was introduced in Section 3.1. Here, kink and antikink approach each other with initial velocity $v_0 = 0.2742$ while vibrating with amplitude $a = 0.015$. Notice, thus, that the first collision is a weakly wobbling kink scattering event. As we know, after this first impact an important part of the kinetic energy is devoted to excite the shape mode and emit radiation, such that the resulting kink and antikink move very slowly but vibrates

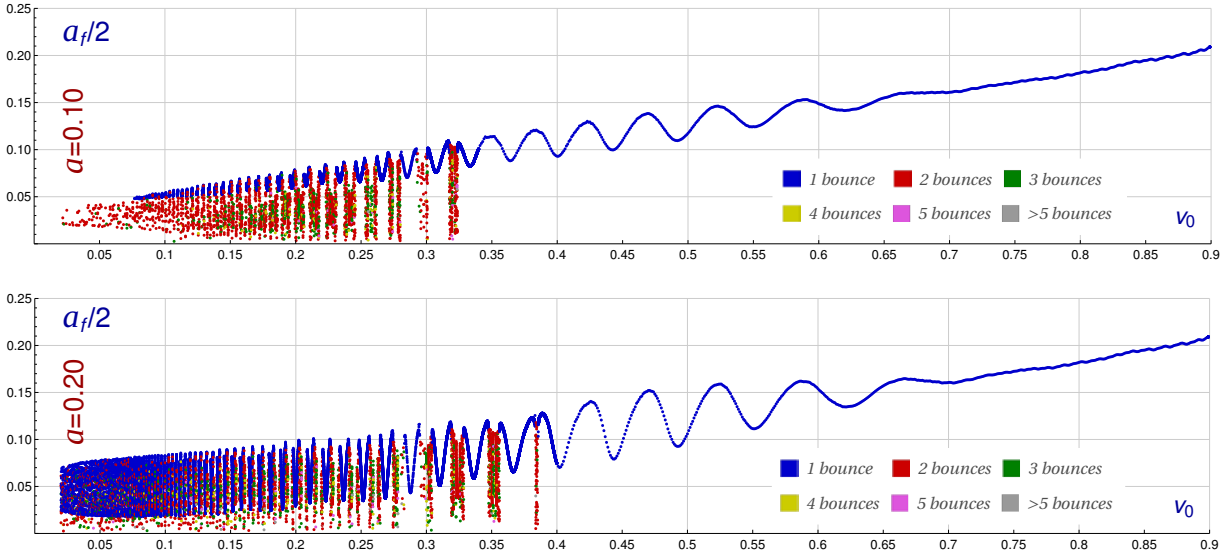

Figure 17: Wobbling amplitude of the scattered kinks after the last impact as a function of the collision velocity v_0 for the initial amplitude $a = 0.1$ (top panel) and $a = 0.2$ (bottom panel). The same color code employed in previous Figures is used to specify the number of bounces suffered by the kinks before escaping.

intensely. In these circumstances the attraction force between the kink and the antikink makes them approach again. This evolution is now described by a strongly wobbling kink scattering event. The lumps collide and bounce back, but now the resonant energy transfer mechanism is reversed and the kink and antikink velocities are large enough to let them escape. They travel away with final velocity $v_f = 0.147041$ and final wobbling amplitude $a = 0.153513$. Figure 11 (right) represents a 3-bounce kink scattering process, where a similar behavior takes place, although the intermediate stages are much shorter. They finally move away with velocity $v_f = 0.219006$ and wobbling amplitude $a = 0.00308$.

The behavior of the final wobbling amplitude a_f as a function of the initial velocity is plotted in Figure 17. The amplitude can undergo important fluctuations when the initial velocity varies, which increases as the value of a grows. These oscillations can be observed, for example, in the 1-bounce reflection tail. The range of the wobbling amplitudes found in these cases is similar to that described in Section 3.1 for weakly wobbling kink scattering processes. The minima of these fluctuations can reach very low values. In the resonance phase these oscillations are more accentuated for these 1-bounce events than in the previous regime. Obviously, the detailed behavior of the amplitude in the resonance phase is completely particular for every value of a due to the presence of the fractal structure.

Besides, the dependence of the final frequency ω_f on the initial velocity v_0 completely resembles the result found in Section 3.1, see Figure 18. Therefore, the final frequency seems to be a magnitude almost independent of the initial wobbling amplitude a beyond the resonance regime.

4 Collective coordinate approach

In the kink-antikink scattering the shape mode plays a fundamental role in the energy transfer mechanism and consequently in the n-bounce kink scattering process and n-bounce windows shown in Section 3. In this section, we focus on an analytical approach to describe the influence of the shape mode and the initial velocity in this process.

In order to have more insight on its dynamical role on the wobbling kink-antikink interaction we make use of the *collective coordinate approach*. This method has been mainly considered in the literature to study scattering of solitons in several models [15, 53, 61, 70, 71, 62]. This approach sheds light on

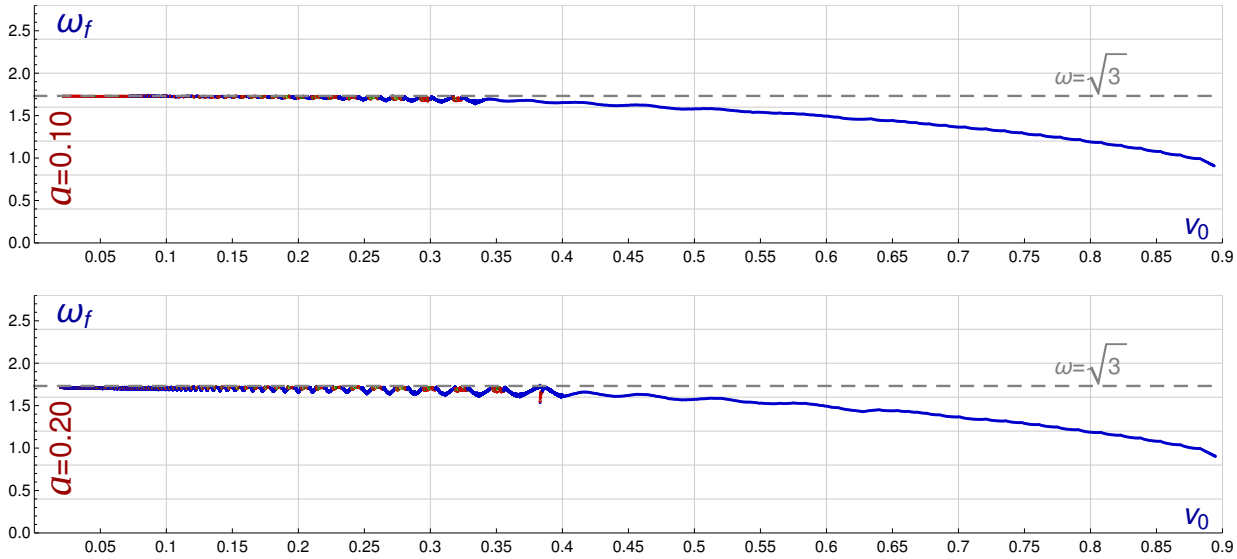

Figure 18: Wobbling frequency of the scattered kinks after the last impact as a function of the collision velocity v_0 for the initial amplitude $a = 0$ (top panel) and $a = 0.02$ (bottom panel). The same color code as in previous figures is used to specify the number of bounces suffered by the kinks before escaping.

the dynamical evolution of the amplitude and the function that describes the separation between kink centers. In reference [61] an ansatz field for the kink-antikink configuration is introduced in the form

$$\phi_{cc}(x,t) = \phi_{\rm K}(\xi_+) - \phi_{\bar{\rm K}}(\xi_-) - 1 + \sqrt{\frac{3}{2}}a(t)\left[\psi_{\omega^2=3}(\xi_+) - \psi_{\omega^2=3}(\xi_-)\right] \quad , \tag{20}$$

with

$$\xi_\pm = \frac{x}{\sqrt{1-v_0^2}} \pm F(t) \quad \text{and} \quad \dot{F}(0) = \frac{-v_0}{\sqrt{1-v_0^2}} \quad , \tag{21}$$

where $a(t)$ is the time-dependent amplitude of the shape mode and $F(t)$ is separation function between the centers of the wobbling kinks. In the literature these collective coordinates have been used extensively to simplify the analytical treatment of kink scattering. The idea behind this change of variables is to map the evolution of the kinks through time dependent coordinates. By doing this one simplifies the partial differential equations to ordinary differential equations. Substituting the ansatz (20) in the Lagrangian density (2) and integrating over all the spatial coordinate we obtain an effective Langrangian in terms of collective coordinates,

$$\begin{aligned} L_{eff}(a,\dot{a},F,\dot{F}) &= \int_{-\infty}^{+\infty} dx\, \mathcal{L}(\partial_\mu\phi_{cc},\phi_{cc}) \\ &= \epsilon_1\dot{F}^2 - \epsilon_2 + \epsilon_3\dot{a}^2 - \epsilon_4 a^2 + \epsilon_5 a + \epsilon_6\dot{F}^2 a + \epsilon_7\dot{F}\dot{a} \\ &\quad + \epsilon_8\dot{F}^2a^2 + \epsilon_9 a\dot{F}\dot{a} + \epsilon_{10}a^3 + \epsilon_{11}a^4 \quad , \end{aligned} \tag{22}$$

where the coefficients in (22) are given by the spatial integration of the Lagrangian density. Take into account all these coefficients would impose considerable difficulty to compute an analytical expression for collective coordinates. For this reason, approximations have been performed through literature, like the harmonic approximation (in this case ϵ_6, ..., $\epsilon_{11} = 0$), in order to circumvent these computation issues. In reference [61] an important contribution was given correcting the term here labeled as ϵ_5, which was mistakenly computed in [13]. Although, this correction was not sufficient to fit simulation data making use of the harmonic approximation.

In a recent study [62] it was shown that including more coefficients in the approximation of collective coordinates produces a better fit of the analytical approach solutions with the numerical simulations outcome. Also, the energy transfer mechanism between zero and shape mode was explained with good precision. For this reason we shall follow the study mentioned before including all terms in (22) with the execption of cubic and quartic terms, since we are studying cases with amplitudes $a \leq 0.2$.

We compactified (22) taking an equivalent Lagrangian density written in terms of coupling functions, a potential-like term and the canonical variables. We choose this procedure because one can see more clearly the influence of the energy in shape mode onto the kinetic energy and vice versa. The equivalent Langrangian density is of the form

$$\bar{\mathcal{L}}(F, \partial_\mu F, a, \partial_\mu a) = f(F,a)\partial_\mu F \partial^\mu F + g(F)\partial_\mu a \partial^\mu a + h(F,a)\partial_\mu F \partial^\mu a - V(F,a) \quad , \tag{23}$$

where the functions multiplying the kinetic and the potential-like terms are given in terms of ϵ_1, ϵ_2, ..., ϵ_9 and the time-dependent amplitude. From the energy momentum tensor for this theory we found the total energy (7) written as

$$\mathrm{E} = f(F,a)\dot{F}^2 + g(F)\dot{a}^2 + h(F,a)\dot{F}\dot{a} + V(F,a) \quad , \tag{24}$$

and the center of mass of the system as

$$\langle x \rangle = \frac{\int x\, E\, dx}{\int E\, dx} \quad . \tag{25}$$

Comparing (23) and (22) we obtain explicitly the coupling functions to be

$$\begin{aligned} f(F,\, a) &= \epsilon_1 + \epsilon_6\, a + \epsilon_8\, a^2, \quad g(F) = \epsilon_3 \quad , \\ h(F,\, a) &= \epsilon_7 + \epsilon_9\, a, \quad V(F,\, a) = \epsilon_5\, a - \epsilon_2 - \epsilon_4\, a^2 \quad . \end{aligned} \tag{26}$$

In Appendix B in [62] one can find how the integral (22) is performed to find ϵ_1, ϵ_2, ..., ϵ_9 using the method of residues, that can be extended to all coefficients. Using these expressions found there we obtain the coupling functions in the equivalent Lagrangian (23) in the form

$$\begin{aligned} f(F,\, a) = {} & \frac{4}{3} + 8\, F \coth(2\, F)\, \mathrm{csch}^2(2\, F) - 4\, \mathrm{csch}^2(2\, F) \\ & + a\, \frac{\pi}{2}\sqrt{\frac{3}{2}}[1 + 2\, \mathrm{sech}^4(F) - \cosh(2\, F)\, \mathrm{sech}^4(F)] \\ & + a^2\, \frac{3}{4}\Big[\frac{28}{15} + 160\, F\, \mathrm{csch}^3(2\, F) + 8\, F\, \mathrm{csch}(2\, F) + 192\, F\, \mathrm{csch}^5(2\, F) \\ & - 96\, \coth(2\, F)\, \mathrm{csch}^3(2\, F) - 16\, \coth(2\, F)\, \mathrm{csch}(2\, F)\Big] \quad , \end{aligned} \tag{27a}$$

$$g(F) = \frac{1}{2}[2 + 12\, F\, \mathrm{csch}(2\, F) + 24\, F\, \mathrm{csch}^3(2\, F) - 12 \coth(2\, F)\mathrm{csch}(2\, F)] \quad , \tag{27b}$$

$$\begin{aligned} h(F,\, a) = {} & \pi\sqrt{\frac{3}{2}}\tanh(F)\, \mathrm{sech}^2(F) + a\, \frac{3}{2}\Big[15\, \mathrm{csch}^3(2\, F) + 9\, \mathrm{csch}(2\, F)\, \coth^2(2\, F) \\ & + 3\, \mathrm{csch}(2\, F) - 6\, F\, \mathrm{csch}(2\, F) \coth(2\, F) - 46\, F\, \coth(2\, F)\mathrm{csch}^3(2\, F) \\ & - 2\, F\, \coth^3(2\, F)\mathrm{csch}(2\, F)\Big] \quad , \end{aligned} \tag{27c}$$

$$\begin{aligned} V(F,\, a) = {} & 8\Big[-\frac{2}{3} + 2\, F + \frac{3}{\tanh(2\, F)} - 2\frac{1 + 3\, F}{\tanh^2(2\, F)} \\ & + \frac{4\, F}{\tanh^3(2\, F)}\Big] - 3\, a^2 - a\, 6\pi\sqrt{\frac{3}{2}}\tanh^2(F)\, [\tanh(F) - 1]^2 \quad . \end{aligned} \tag{27d}$$

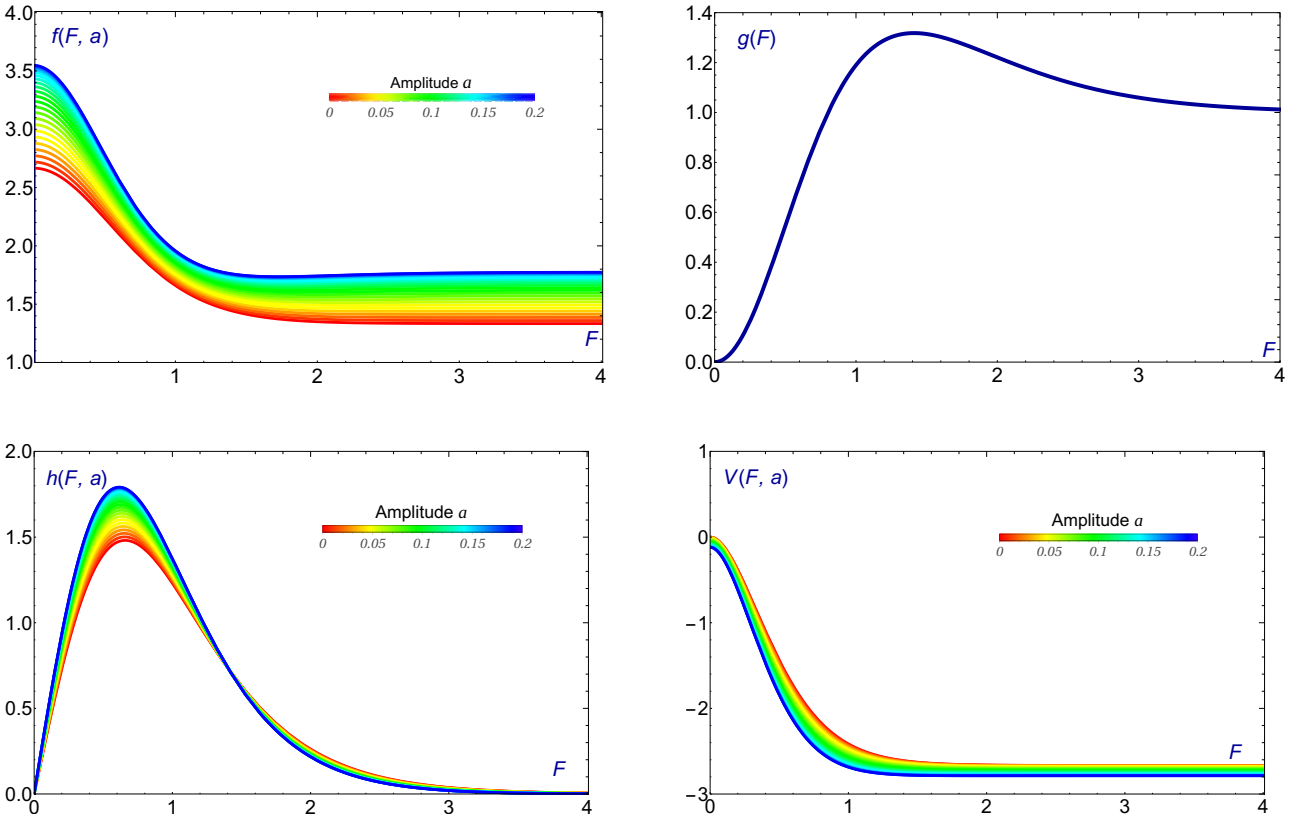

Figure 19: Coupling functions in terms of the separation function F. The initial amplitude influence onto the coupling functions is highlighted. When kink-antikink solutions are far apart from each other the coupling functions are assumed to be constant varrying in value according to the inital amplitude.

The behavior of these coupling functions can be seen in Figure 19. Note that the energy transfer mechanism mediated by the coupling function $h(F, a)$ is different of zero when the solutions are about to collide and goes to zero when the solutions are found to be at the origin where the energy is all stored in the translational mode, that is where maximum of $f(F, a)$ and minimum of $g(F)$ occurs. After the scattering process the kinetic energy is slowly released to the vibrational mode reaching a constant value that depends on the inital values of amplitude and velocity. It is also worthwhile to mention that the potential-like term in (23) is negative before collision, even for large initial values of $F(0)$, in accordance with the attractive force acting on the kinks. This means that even if kink-antikink solution are far apart with zero initial relative velocity to each other they are still under an attractive force that make the kink-antikink collide after long enough time. Moreover, one can see in Figure 19 that for the greater initial amplitude is the stronger the attractive force is.

From (23) we obtain the equations of motion for the collective parameters given by

$$\partial_\mu \left[\frac{\partial \bar{\mathcal{L}}}{\partial(\partial_\mu a)}\right] - \frac{\partial \bar{\mathcal{L}}}{\partial a} = 0 \quad , \quad \partial_\mu \left[\frac{\partial \bar{\mathcal{L}}}{\partial(\partial_\mu F)}\right] - \frac{\partial \bar{\mathcal{L}}}{\partial F} = 0 \quad , \tag{28}$$

that leads, respectively, to

$$2\, f\, \ddot{F} + h\, \ddot{a} + \dot{F}(f_F\, \dot{F} + 2\, f_a\, \dot{a}) + \dot{a}^2\, (h_a - g_F) + V_F = 0 \quad , \tag{29a}$$

$$2\, g\, \ddot{a} + h\, \ddot{F} + \dot{F}\, (h_{_F}\, \dot{F} + 2\, g_F \dot{a} - f_a\, \dot{F}) + V_a = 0 \quad , \tag{29b}$$

where $f_F = \frac{\partial f}{\partial F}$ and $f_a = \frac{\partial f}{\partial a}$. We can see that these strongly coupled ordinary differential equations preserve the total energy of the configuration over all time. In the following graphs we show some

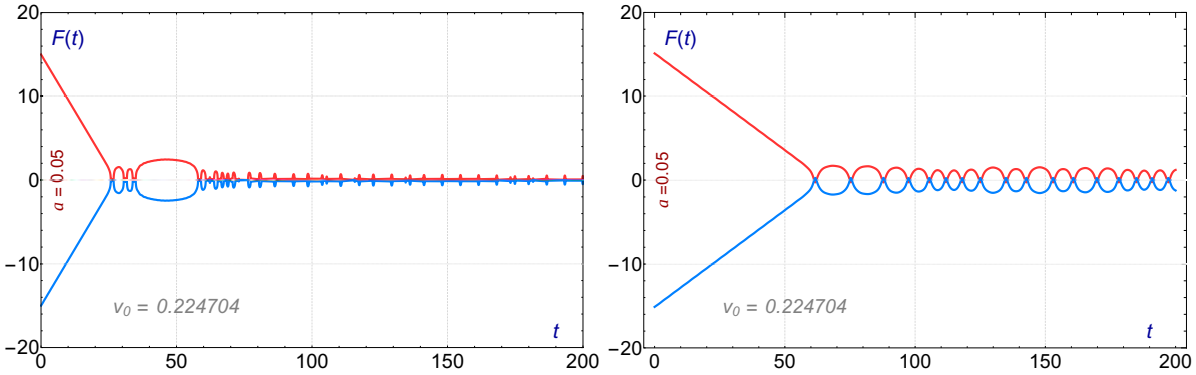

Figure 20: In this graph one can see the behaviour of the distance between the centers of the topological defects $F(t)$ as a function of time for the numerical simulation outcome (*left*) and the numerical solution to the collective coordinate approach (*right*). A bion formation is observed in the resonance regime for intial amplitude $a = 0.05$ and initial velocity $v = 0.224704$. As in the numerical simulation the energy is slowly dissipated to space in form of radiation.

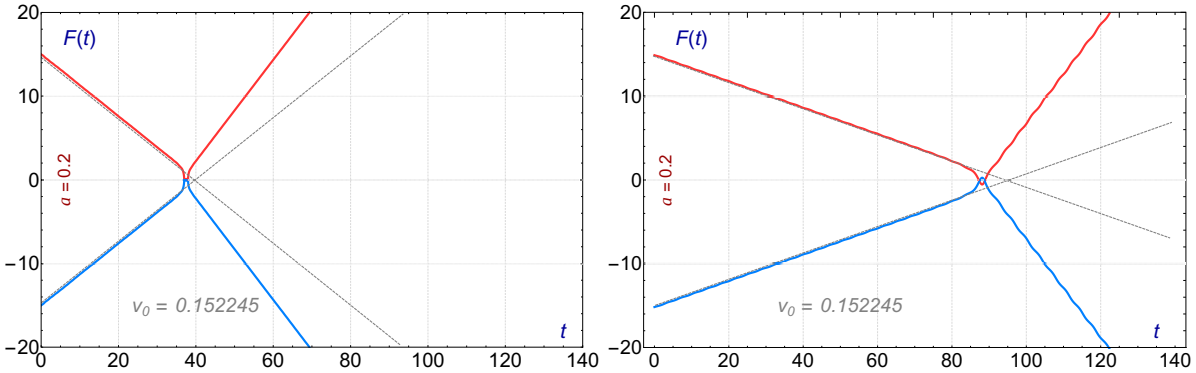

Figure 21: In this graph, one can see that for large initial amplitudes the scattered solutions moves away with bigger velocity than the one before the interaction. In this scenario the final amplitude is considerable smaller the the initial one.

numerical solutions to equations (29) for the ansatz $a = a_0 \sin(\sqrt{3}\,t)$ and the outcome of the numerical simulations for the respective initial amplitude and velocity. In these results, we can see that the numerical solutions of the collective coordinates reproduce the patterns of the simulation outcome with reasonable approximation, see, for instance, Figure 20 that shows a bion formation in the resonance regime.

Its worthwhile to mention that at the collision point the centers of the wobbling kink and wobbling antikink pass through each other and then bounce back in the numerical solutions for collective coordinates approach. In Figure 21, we can see that for large initial amplitude, and low enough initial velocities, the scattered topological defects moves away with final velocity bigger than the initial one. In this case the amount of energy in the vibrational mode released to the translational mode is big enough to make the solutions split away with great velocity. This is a new particular result of scattering between topological defects. We argue that for initial amplitudes $a > 0.2$ this configuration becomes prevalent. When the solutions approach the collision point, their speed grows exponentially in accordance with the behaviour of the kinetic term $f(F, a)$, that can be seen in Figure 19. In the collision point all the enery of the configuration is stored in the kinetic term and when the solutions bounce back the energy is slowly released to the vibrational mode.

5 Conclusions and further comments

In this paper we have addressed the scattering between wobbling kinks in the ϕ^4 model. In addition to its intrinsic interest the study of these processes can give us insight into the resonant energy transfer mechanism. We must take into account that two traveling non-excited kinks become wobbling kinks after the first collision due to the energy exchange between the translational mode and the shape mode. In this sense, a n-bounce scattering process can be considered as the reiteration of n 1-bounce collisions, most of them between wobbling kinks. In this work the influence of the collision velocity and the initial wobbling amplitude on the scattering processes have been directly investigated. The fractal structure arising in the resonance regime of the final versus initial velocity diagram becomes more intricate as the value of the initial wobbling amplitude of the colliding kinks increases. This growing complexity is caused by two different mechanisms: the 1-bounce reflection tail splitting and the spontaneous emergence of resonance windows. The first case is produced by the oscillations of the 1-bounce reflection tail when the initial wobbling amplitude grows. When the amplitude is large enough this curve can intercept the v_0-axis creating an isolated 1-bounce window in the resonance regime. The gap between this new window and the 1-bounce tail is filled with new n-bounces windows, with $n > 1$. The same phenomenon is replicated for n-bounce windows, which are broken up into narrower new n-bounce windows and as before the gap between them is occupied with N-bounce windows, with $N > n$. The second mechanism is directly triggered by the extra energy carried by the initially excited shape mode of the wobbling kinks. New bounce windows emerge for ever-smaller initial velocities as the value of the amplitude increases. As a consequence, the fractal structure interval becomes larger and larger as a grows. On the other hand, the final wobbling amplitude of the scattered kinks involve a very approximately linear dependence on the initial velocity outside the resonance phase although some oscillations arise for large enough values of the initial amplitude. 1-bounce events between weakly wobbling kinks always give rise to strongly wobbling kinks moving away. On the other hand, weakly wobbling kinks can emerge from the collision between strongly wobbling kinks only for relatively small values of the initial velocity. A surprising result is that the frequency of the shape mode is a decreasing function of the collision velocity starting from the natural frequency $\omega = \sqrt{3}$ found in the linear analysis. This curve is almost independent of the value of the initial wobbling amplitude.

It is worthwhile to mention that for strongly wobbling kink collisions there exist 1-bounce windows where the scattered kinks will travel faster than the colliding kinks. This occurs for relatively low values of the initial velocity. This behavior implies that the last collision in every n-bounce scattering event with $n > 1$ must involve the presence of strongly wobbling kinks approaching each other at a relatively low speed. In a multiple bounce scattering process the kinks approach each other and bounce back again and again until the next collision velocity and wobbling amplitude fall into one of the previously mentioned 1-bounce windows. In the bion formation regime the successive collisions are not able to excite the shape mode enough to trigger this escape manoeuvre.

The *collective coordinate method* introduced in Section 4 shows that the amplitude of the shape mode plays a fundamental role in the dynamics of the wobbling kinks. The distance between the kink centers and the wobbling amplitude constitute the independent canonical variables of the finite-dimensional effective Lagrangian (22). The interaction is governed by coupling functions for well separated kinks that assume constant values, which change slightly with the amplitude. The behavior of those coupling functions reveals that when the solutions are found to be at the origin all the energy is stored in translational mode and the attractive force between them reach approximately to zero. In a n-bounce scattering event the energy is slowly released to vibrational mode, reaching a constant value that depends on the collision velocity and the initial magnitude of the excited state.

The research introduced here open some possibilities for future works. The ϕ^6 model involves a similar resonance regime as the ϕ^4 model although it does not present vibrational eigenstates in the second order

small fluctuation operator. The characteristics of the scattered wobbling kinks can be analyzed to study its influence on the resonant energy transfer mechanism. Alternatively, a twin model to the ϕ^6 model involving internal modes can be constructed. By doing this, we could compare the scattering processes of the twin model with those of the standard ϕ^6 model. In this way the role played by the shape modes in the collision process could be examined. Moreover, many other different topological defects (kinks in the double sine-Gordon model, deformed ϕ^4 models, hybrid and hyperbolic models, etc) could be studied in the new perspective presented here.

Acknowledgments

A. Alonso-Izquierdo acknowledges the Junta de Castilla y León for financial support under grants BU229P18 and SA067G19. J.V. Queiroga-Nunes aknowledges for financial support of Santander Group under scholarship program UVa - Santander Iberoamerica+Asia. This research has made use of the high performance computing resources of the Castilla y León Supercomputing Center (SCAYLE, www.scayle.es), financed by the European Regional Development Fund (ERDF).

References

[1] A. R. Bishop, J.A. Krumhansl and S.E. Trullinger, Physica D **1**, 1 (1980).

[2] A.H. Eschenfelder, *Magnetic Bubble Technology* (Springer-Verlag, Berlin, 1981).

[3] F. Jona and G. Shirane, *Ferroelectric Crystals* (New York, Dover, 1993).

[4] B.A. Strukov and A.P. Levanyuk, *Ferroelectric Phenomena in Crystals: Physical Foundations* (Springer-Verlag, Berlin, 1998).

[5] A. Vilenkin and E.P.S. Shellard, *Cosmic strings and other topological defects* (Cambridge University Press, Cambrigde, UK, 1994).

[6] T. Vachaspati, *Kinks and Domain walls: An Introduction to classical and quantum solitons* (Cambridge University Press, Cambrigde, UK, 2006).

[7] L.F. Mollenauer and J.P. Gordon, *Solitons in optical fibers - Fundamentals and applications* (Academic Press, Burlington, 2006).

[8] T. Schneider, *Nonlinear optics in Telecommunications* (Springer, Heidelberg, 2004).

[9] G.P. Agrawall, *Nonlinear Fiber Optics* (Academic Press, San Diego, 1995).

[10] A. S. Davydov, *Solitons in molecular systems* (D. Reidel, Dordrech, 1985).

[11] D. Bazeia and E. Ventura, Chem. Phys. Lett. **303**, 341 (1999).

[12] L.V. Yakushevich, *Nonlinear Physics of DNA* (Wiley-VCH, Weinheim, 2004).

[13] T. Sugiyama, Progr. Theoret. Phys. **61**, 1550 (1979).

[14] D. K. Campbell, J. S. Schonfeld and C. A. Wingate, Phys. D **9**, 1 (1983).

[15] P. Anninos, S. Oliveira and R.A. Matzner, Phys. Rev. D **44**, 1147 (1991).

[16] J. Shiefman and P. Kumar, Phys. Scr. **20**, 435 (1979).

[17] M. Peyrard and D. K. Campbell, Physica D **9**, 33 (1983).

[18] D.K. Campbell, M. Peyrard and P. Sodano, Physica D **19**, 165 (1986).

[19] V.A. Gani and A.E. Kudryavtsev, Phys. Rev. E **60**, 3305 (1999).

[20] B. A. Malomed, Phys. Lett. A **136**, 395 (1989).

[21] V.A. Gani, A.M. Marjaneh, A. Askari, E. Belendryasova and D. Saadatmand, Eur. Phys. J. C **78**, 345 (2018).

[22] F.C. Simas, A.R. Gomes, K.Z. Nobrega and J.C.R.E. Oliveira, JHEP **9**, 104 (2016).

[23] A.R. Gomes, F.C. Simas, K.Z. Nobrega and P.P. Avelino, JHEP **10**, 192 (2018).

[24] D. Bazeia, E. Belendryasova and V.A. Gani, J. Phys.: Conf. Ser. **934**, 012032 (2017).

[25] D. Bazeia, E. Belendryasova and V.A. Gani, Eur. Phys. J. C **78**, 340 (2018).

[26] D. Bazeia, A.R. Gomes and K.Z. Nobrega, Int. J. of Modern Physics A **34**, 31 (2019).

[27] C. Adam, K. Oles, T. Romanczukiewicz and A. Wereszczynski, Phys. Rev. Lett. **122**, 241601 (2019).

[28] T. Romanczukiewicz and Y. Shnir, *Some recent developments on kink collisions and related topic: A Dynamical Perspective on the ϕ^4 Model* (Springer, Cham, 2019).

[29] T. Romanczukiewicz, Phys. Lett. B **773**, 295 (2017).

[30] H. Weigel, J. Phys.: Conf. Ser. **482**, 012045 (2014).

[31] V.A. Gani, A.E. Kudryavtsev and M.A. Lizunova, Phys. Rev. D **89**, 125009 (2014).

[32] D. Bazeia, A.R. Gomes, K.Z. Nobrega and F.C. Simas, Phys. Lett. B **793**, 26 (2019).

[33] F.C. Lima, F.C. Simas, K.Z. Nobrega and A.R. Gomes, JHEP **10**, 147 (2019).

[34] T. S. Mendonça and H. P. de Oliveira, Braz. J. Phys. **49**, 914 (2019).

[35] Y. Zhong, X.L. Du, Z.C. Jiang, Y.X, Liu and Y.Q. Wang, JHEP **02**, 153 (2020).

[36] D. Bazeia, A.R. Gomes, K.Z. Nobrega and F.C. Simas, Phys. Lett. B **803**, 135291 (2020).

[37] A. Halavanau, T. Romanczukiewicz and Ya. Shnir, Phys. Rev. D **86**, 085027 (2012).

[38] T. Romanczukiewicz, Acta Phys. Polon. B **39**, 3449 (2008).

[39] A. Alonso-Izquierdo, Phys. Rev. D **97**, 045016 (2018).

[40] A. Alonso-Izquierdo, Phys. Scr. **94**, 085302 (2019).

[41] A. Alonso-Izquierdo, Physica D: Nonlinear Phenomena **365**, 12 (2017).

[42] A. Alonso-Izquierdo, Commun. Nonlinear Sci. Numer. Simulat. **75**, 200 (2019).

[43] A. Alonso-Izquierdo, Commun. Nonlinear Sci. Numer. Simulat. **85**, 105251 (2020).

[44] L.A. Ferreira, P. Klimas and J. Zakreswski, JHEP **01**, 020 (2019).

[45] Z. Fei, Y. Kivshar and L. Vazquez, Phys. Rev. A **45**, 6019 (1992).

[46] Z. Fei, Y. S. Kivshar and L. Vazquez, Phys. Rev. A **46**, 5214 (1992).

[47] R.H. Goodman, P.J. Holmes and M.I. Weinstein, Physica D **161**, 21 (2002).

[48] R. H. Goodman and R. Haberman, Phys. D **195**, 303 (2004).

[49] B.A. Malomed, Physica D: Nonlinear Phenomena **15**, 385 (1985).

[50] B. A. Malomed, J. Phys. A: Math. Gen. **25**, 755 (1992).

[51] K. Javidan, J. Phys. A: Math. Gen. **39**, 10565 (2006).

[52] D. Saadatmand and K. Javidan, Phys. Scr **85**, 025003 (2012).

[53] D. Saadatmand and K. Javidan, Braz. J. Phys. **43**, 48 (2013).

[54] D. Saadatmand, S.V. Dmitriev, D.I. Borisov, P.G. Kevrekidis, M.A. Fatykhov and K. Javidan, Commun. Nonlinear. Sci. Numer. Simulat. **29**, 267 (2015).

[55] D. Saadatmand, D.I. Borisov, P.G. Kevrekidis, K. Zhou and S.V. Dmitriev, Commun. Nonlinear. Sci. Numer. Simulat. **56**, 62 (2018).

[56] C. Adam, T. Romanczukiewicz and A. Wereszczynski, JHEP **3**, 131 (2019).

[57] C. Adam, K. Oles, J.M. Queiruga, T. Romanczukiewicz and A. Wereszczynski, JHEP **07**, 150 (2019).

[58] P. Dorey, K. Mersh, T. Romanczukiewicz and Y. Shnir, Phys. Rev. Lett. **107**, 091602 (2011).

[59] P. Dorey and T. Romanczukiewicz, Phys. Lett. B **779**, 117 (2018).

[60] J.G.F. Campos and A. Mohammadi, Eur. Phys. J. C. **80**, 352 (2020).

[61] I. Takyi and H. Weigel, Phys. Rev. D **94**, 085008 (2016).

[62] C.F.S. Pereira, G. Luchini, T. Tassis and C.P. Constantinidis, arXiv:2004.00571v2.

[63] B. S. Getmanov, JETP Lett. **24**, 291 (1976).

[64] I.V. Barashenkov and O.F. Oxtoby, Phys. Rev. E **80**, 026608 (2009).

[65] I.V. Barashenkov, *A Dynamical Perspective on the ϕ^4 Model: The Continuing Story of the Wobbling Kink* (Springer, Cham, 2019), 187-212.

[66] H. Segur, J. Math. Phys. **24**, 1439 (1983).

[67] N.S. Manton and H. Merabet, Nonlinearity **10**, 3 (1997).

[68] A.K. Kassam and L. N. Trefethen, SIAM J. Sci. Comp. **26**, 1214 (2005).

[69] S. Cox, P. Matthews and J. Cumput. Phys. **176**, 430 (2002).

[70] R.H. Goodman and R. Haberman, SIAM J. Appl. Dyn. Syst. **4**, 1195 (2005).

[71] I. Takyi, MSc. thesis, Stellenbosch University, 2015, http:// scholar.sun.ac.za/handle/10019.1/97877.